


Experimental hierarchy and optimal robustness of quantum correlations of two-qubit states with controllable white noise

Kateřina Jiráková ^{1,*}, Antonín Černocho ^{2,†}, Karel Lemr ^{1,‡}, Karol Bartkiewicz ^{1,3,§} and Adam Miranowicz ^{3,||}

¹*Joint Laboratory of Optics of Palacký University and Institute of Physics of Czech Academy of Sciences, 17. listopadu 12, 779 00 Olomouc, Czech Republic*

²*Institute of Physics of the Czech Academy of Sciences, Joint Laboratory of Optics of PU and IP AS CR, 17. listopadu 50A, 772 07 Olomouc, Czech Republic*

³*Institute of Spintronics and Quantum Information, Faculty of Physics, Adam Mickiewicz University, 61-614 Poznań, Poland*

 (Received 5 March 2021; revised 1 September 2021; accepted 2 December 2021; published 21 December 2021)

We demonstrate a hierarchy of various classes of quantum correlations on experimentally prepared two-qubit Werner-like states with controllable white noise. Werner states, which are white-noise-affected Bell states, are prototypical examples for studying such a hierarchy as a function of the amount of white noise. We experimentally generate Werner states and their generalizations, i.e., partially entangled pure states affected by white noise. These states enable us to study the hierarchy of the following classes of correlations: separability, entanglement, steering in three- and two-measurement scenarios, and Bell nonlocality. We show that the generalized Werner states (GWSs) reveal fundamentally different aspects of the hierarchy compared to the Werner states. In particular, we find five different parameter regimes of the GWSs, including those steerable in a two-measurement scenario but not violating Bell inequalities. This regime cannot be observed for the usual Werner states. Moreover, we find threshold curves separating different regimes of the quantum correlations and find the optimal states which allow for the largest amount of white noise which does not destroy their specific quantum correlations (e.g., unsteerable entanglement). Thus, we could identify the optimal Bell-nondiagonal GWSs which are, for this specific meaning, more robust against the white noise compared to the Bell-diagonal GWSs (i.e., Werner states).

DOI: [10.1103/PhysRevA.104.062436](https://doi.org/10.1103/PhysRevA.104.062436)

I. INTRODUCTION

A. Entanglement, steering, and Bell nonlocality

Quantum entanglement [1] and its generalizations, i.e., quantum steering [2,3] and Bell nonlocality [4], are fundamental types of quantum correlations between spatially separated systems (parties). These effects reveal the disparity between classical and quantum physics from a fundamental point of view, but also play a pivotal role in quantum information and its applications in quantum technologies of second generation [5–8]. (i) Quantum entanglement (or quantum inseparability) occurs when the state of one party cannot be described independently of the state of the other party [5]. (ii) Quantum steering, also referred to as Einstein-Podolsky-Rosen (EPR) steering, refers to the ability of one party (say, Alice) to affect the state of the other party (say, Bob) through the choice of her measurement basis, which cannot be explained by any local hidden state (LHS) models [7,8]. Moreover, (iii) quantum nonlocality can be defined as the effect detectable by the violation of the Bell inequality and thus which cannot be explained by any local hidden variable (LHV) models. Here we limit our interest to the two-qubit

Bell inequality in the Clauser-Horne-Shimony-Holt (CHSH) form [9]. Thus, we refer to this effect as Bell(-CHSH) nonlocality, having in mind that quantum nonlocality can also be understood in a much broader sense [6].

The distinction between these effects is fundamental, and their intuitive operational interpretation can be given from a measurement perspective, i.e., by referring to their detection using two types of measuring devices, which can be perfect or imperfect from physical and technological points of view or trusted or untrusted from a cryptographic perspective, i.e., with or without prior knowledge about the devices [10]. Specifically, (i) quantum entanglement between two systems can be detected using trusted devices for both systems, (ii) EPR steering can be tested by trusted devices for one system and untrusted ones for the other, and (iii) quantum nonlocality can be detected by untrusted devices on both sides. Such interpretation has direct applications for quantum cryptology, including secure communication. In the same measurement scenarios, Bell nonlocality implies steering and steering implies entanglement, but not vice versa, in general. Indeed, there exist entangled [11] and steerable states which do not violate Bell inequalities as well as unsteerable entangled states [7,8].

B. Werner states and their experimental generation

Mixtures of a Bell state and a maximally mixed state (i.e., white noise) are prototypical examples of states revealing the nonequivalence of entanglement and Bell nonlocality, which

*katerina.jirakova@upol.cz

†acernoch@fzu.cz

‡k.lemr@upol.cz

§karol.bartkiewicz@upol.cz

||miran@amu.edu.pl

was first demonstrated by Werner over 30 years ago [11]. The Werner states were later used to show a hierarchy of criteria and a hierarchy of some classes of correlations (CC) (which for short is here referred to as CC hierarchy), including quantum steering (see, e.g., reviews in [5–8] and the very recent work in Ref. [12] with references therein). The effect of white noise on Bell states has also been studied theoretically to reveal a hierarchy of the following classes of temporal quantum correlations [13]: temporal inseparability [14], violations of temporal Bell-CHSH inequalities [15], and temporal steering [16,17].

We stress that we only consider von Neumann’s projective measurements in this work. Note that the quantum-correlation regimes of states assumed for projective measurements are different from those based on positive-operator-valued measures (POVMs). However, the same hierarchy relations, as studied here, still hold assuming POVMs.

Generation of mixed states of discrete photons has been investigated both theoretically [18–20] and experimentally [21–34]. Temporal decoherence of optical polarization modes in a birefringent material seems to be a rather widely used technique in a number of experiments such as those reported in Refs. [25,34]. This technique has also enabled the experimental generation of maximally entangled mixed states (MEMSs) [35] by Peters *et al.* [32] and later by Aiello *et al.* [30]. Recently, Liu *et al.* incorporated a tunable decoherence channel [36] to generate the Werner states [23]. Alternative methods to generate or simulate temporal decoherence include the generation of mixed states by exploiting a particular geometry of a spontaneous parametric down-conversion (SPDC) source [21,31]. Barbieri *et al.* [33] and Cinelli *et al.* [27] reported their refined two-photon sources capable of preparing a broad range of mixed quantum states, including MEMSs. A highly birefringent material, together with a wide momentum spectrum of generated photon pairs (resulting in effective spatial decoherence), was also used as an alternative method to generate temporal decoherence [25]. Puentes *et al.* applied wedge depolarizers and bucket detectors [24] and later utilized scattering in various media [29]. Moreover, Zhang *et al.* incoherently combined photons generated in two separate SPDC sources to create mixed quantum states [26], while Caminati *et al.* reported an experiment where mixed states were generated by attenuating a high-gain SPDC source [28]. The idea of using a wide-temporal detection window, such that a detected state appeared to be mixed, was also implemented in several experiments [22,37]. It is also possible to use an experimental setup that can be tuned (to change properties of generated states) in times shorter than the measurement integration time [38].

In this work we report experimental generation of both Werner states and their generalizations, i.e., partially entangled pure states affected by white noise, which we refer to as generalized Werner states (GWSs). These states were not the focus of the above-reviewed experiments. Some of the experimental setups cannot generate these generalized states (e.g., Ref. [30]), some could be used after specific improvements (e.g., Ref. [23]), and the others might have such capabilities, but these (e.g., Ref. [26]) have not been used so far for demonstrating the CC hierarchy of the Werner states or their generalizations. In this paper our experimen-

tally generated and reconstructed states are applied to reveal a CC hierarchy.

The remainder of the paper is organized as follows. Two approaches to study hierarchies of correlations are specified in Sec. II. Measures of quantum correlations of general two-qubit states are recalled in Sec. III. These include popular measures of entanglement, steering, and Bell nonlocality. Moreover, steering in the two-, three-, and multimeasurement scenarios is explicitly discussed in Appendices C, B, and D, respectively. In Sec. IV we define GWSs. Because GWSs are a direct generalization of the usual Werner states based on a Bell state, we refer to them as Bell-nondiagonal GWSs. Our experiment is described in Sec. IV. We compare various predictions of the quantum correlations for the theoretical and experimental GWSs with those for the Werner states in Sec. V. We also discuss fundamental differences in a CC hierarchy for the Bell-diagonal and -nondiagonal GWSs in this section. In Sec. VI we present our most counterintuitive theoretical results. Specifically, we show in Sec. VIA that there exist GWSs which are steerable in a two-measurement scenario (2MS) but still admit LHV models. Such a regime cannot be observed for the standard Werner states. In Sec. VIB we show that some Bell-nondiagonal GWSs are more robust against white noise than the diagonal GWSs, i.e., the Werner states. In Sec. VIC we analyze lower and upper bounds on steering for a large number of measurements. We show better robustness against the white noise of unsteerable entangled Bell-nondiagonal GWSs compared to the diagonal ones. An example of a hierarchy of entanglement criteria is discussed in Appendix E in comparison with the CC hierarchy for the GWSs. We conclude in Sec. VII.

II. TWO APPROACHES TO STUDY A HIERARCHY OF QUANTUM CORRELATIONS

Here we study a CC hierarchy, which is the hierarchy of states with different correlation properties rather than types of probability distributions, as in the case of certain research in quantum information. We use the term correlation of a state by referring to its entanglement, steering, and Bell nonlocality. For clarity, we recall that (a) an entangled (separable) state is a state that cannot (can) be factored into individual states belonging to separate subspaces, (b) an EPR steerable (unsteerable) state is the one described by the statistics which cannot (can) be reproduced by an LHS model for a given measurement set (see Sec. IIIB for more details), and (c) a quantum nonlocal (local) state is the one described by the statistics which cannot (can) be reproduced by an LHV model, which in turn implies the violation (fulfillment) of a Bell inequality. Since we are focused on analyzing two-qubit states, the Bell inequalities can be limited to the CHSH inequality. Moreover, the steerability of states can be considered in the limit of an infinite number of measurements, but it is usually limited to practical resources, including a finite number of measurements. We focus in this paper on the GWSs which are steerable or unsteerable in 2MSs and 3MSs, corresponding respectfully to measuring two or three Pauli operators. Thus, we can consider subclasses of steerable states depending on the number of performed measurements. In what follows, we study in detail the hierarchy of correlation classes limited to

analyzing the states which are (i) separable, (ii) entangled but unsteerable in 3MSs, (iii) steerable in 3MSs but not in 2MSs, (iv) 2MS steerable but local, and (v) nonlocal. The hierarchy is extended in Sec. VIC to include the analysis of the GWSs which are steerable for a larger number n of measurements (i.e., $n = 136$).

In general, a hierarchy of quantum correlations can be understood in several ways including (i) a hierarchy of conditions (or criteria) for the observation of a given class of quantum correlations and (ii) a hierarchy of different classes of quantum correlations (i.e., a CC hierarchy). This division is also closely related to experimental demonstrations of a hierarchy by measuring (nonuniversal or universal) witnesses of quantum correlations corresponding to performing partial or full quantum state tomography (QST), respectively.

In this work we focus on analyzing a CC hierarchy of the GWSs. We demonstrate different kinds of quantum correlations in question by performing full QST and then calculating the corresponding measures on the reconstructed states.

Below we explain the main differences between the two approaches to study a hierarchy of quantum correlations and explain why a complete experimental demonstration of the studied CC hierarchy seems to be very challenging within the present state of the art.

A. Hierarchy of criteria for a given class of quantum correlations

Experimental demonstrations of Bell nonlocality via the violations of the CHSH inequalities have been at the heart of quantum information since its early days starting from the pioneering experiments of Aspect *et al.* [39] and then refined in hundreds of experiments, including significant-loophole-free tests (see, e.g., [40–42] and the review in [6] for references). Thus, if one talks about “demonstrating” the nonlocality of a quantum state, one would normally expect to see a violation of a Bell inequality, rather than QST. However, this approach usually reveals only a hierarchy of criteria (i.e., either sufficient or necessary conditions) for the observation of a specific class of quantum correlations. This is because it is usually based on measuring nonuniversal witnesses of quantum correlations by testing the violation of specific inequalities. Note that nonuniversal witnesses correspond usually to *sufficient but not necessary conditions* of a specific quantum (temporal or spatial) correlation effect. Thus, such a witness can usually be determined *without* a complete QST.

Within this hierarchy approach, one can analyze a hierarchy of, e.g., different Bell inequalities or even the Bell-CHSH inequalities but for different angles of polarizers in a description of Bell nonlocality, specifically, by choosing different angles ϕ_1 , ϕ_2 , ϕ'_1 , and ϕ'_2 as described in Eq. (4). By having *a priori* information about a given generated state, one can choose optimal angles of the polarizers to maximize the violation of the Bell-CHSH inequalities and thus to be able to quantify Bell nonlocality (i.e., to determine a nonlocality measure) for the state. However, without knowing *a priori* a given state, one has to measure many copies of the state at different angles of the polarizers to find their optimal rotation. Such scanning of the angles corresponds to (complete or partial) QST.

The hierarchy of criteria has also been studied based on the matrices of the moments of, e.g., the annihilation and creation operators of bosonic or fermionic states of any dimension. Indeed, a number of works demonstrated (i) a hierarchy of sufficient conditions for observing entanglement (i.e., entanglement witnesses) which include the conditions based on the Shchukin-Vogel criterion [43,44] which are related to the Peres-Horodecki criterion and its generalized versions using positive maps beyond partial transpose [45], (ii) a hierarchy of sufficient conditions for observing quantum steering (i.e., steering witnesses) [46], (iii) a hierarchy of necessary conditions for revealing Bell nonlocality (i.e., nonlocality requirements) [47], and (iv) a hierarchy of sufficient conditions for observing spatial [48] and spatiotemporal [49,50] nonclassicality (i.e., nonclassicality witnesses).

An illustrative detailed example of a hierarchy of entanglement criteria is discussed in Appendix E. Note that the upper and lower bounds of measures of quantum correlations, which correspond to their sufficient and necessary conditions, can be determined using such a hierarchy of matrices of moments without a complete QST. However, for an unknown state, to make these bounds tight to a true measure, one needs to increase the number of moments to be detected. This in turn leads to a partial moment-based QST, which approaches more and more a complete QST as explained in Appendix E 3. In conclusion, this approach, in general, enables a direct but partial demonstration of a hierarchy, which is discussed below.

B. Hierarchy of various classes of correlations

A hierarchy of various classes of correlations can be revealed by their measures or by the conditions which are both necessary and sufficient for their observation. It should be stressed that we are focused on demonstrating such a CC hierarchy in this paper.

Indeed, experimental methods for a complete demonstration of a CC hierarchy can be based on experimentally reconstructed density matrices (in the case of standard single-time spatial correlations) or the Choi-Jamiołkowski matrices (in the case of temporal correlations) for a given system via quantum state or process tomographies, respectively. This approach enables the calculation of necessary and sufficient conditions for observing and quantifying the amount of any class of quantum temporal or spatial correlations for a given state or process.

Experimental demonstration of such a CC hierarchy has usually been done using a complete QST, although it can also be done with an incomplete QST, as discussed in Appendix A. Here we apply an indirect approach based on experimental detecting and reconstructing states via a full QST and only then calculating their correlation measures on the reconstructed states. This approach has important fundamental and experimental advantages, which include the following (in addition to the above-mentioned ones).

(i) We want to test the above-mentioned five classes of quantum correlations on the same footing (preferably using the same setup) based on either complete or incomplete tomography. However, it is seen that we can determine experimentally the Horodecki nonlocality measure without QST, but detecting the negativity and the steerable weights (or,

equivalently, steering robustness) can be done effectively only via a complete QST.

(ii) We want to use the same experimental states for testing different quantum properties. The problem is that we do not have perfect control of especially the mixing parameter determining the amount of white noise in a pure state. Thus, we cannot generate the same GWSs even using the same setup. Such a state generation would be even more demanding using different setups for testing different classes of correlations. However, this is feasible using a full QST to reconstruct a state, which is only then numerically studied for its quantum correlations.

III. MEASURES OF QUANTUM CORRELATIONS OF GENERAL TWO-QUBIT STATES

As a part of our introduction, we shortly recall standard measures of quantum correlations for general two-qubit states ρ , which can be written in the Bloch representation as

$$\rho = \frac{1}{4} \left(I \otimes I + \mathbf{u} \cdot \boldsymbol{\sigma} \otimes I + I \otimes \mathbf{v} \cdot \boldsymbol{\sigma} + \sum_{n,m=1}^3 T_{nm} \sigma_n \otimes \sigma_m \right), \quad (1)$$

where $u_i = \text{Tr}[\rho(\sigma_i \otimes I)]$ and $v_i = \text{Tr}[\rho(I \otimes \sigma_i)]$ are the elements of the Bloch vectors $\mathbf{u} = [u_1, u_2, u_3]$ and $\mathbf{v} = [v_1, v_2, v_3]$ of the first and second qubits, respectively, and I is the single-qubit identity operator. Moreover, the correlation matrix elements $T_{ij} = \text{Tr}[\rho(\sigma_i \otimes \sigma_j)]$ and $\boldsymbol{\sigma} = [\sigma_1, \sigma_2, \sigma_3] \equiv [X, Y, Z]$ are expressed via the Pauli matrices.

A. Entanglement measures

Here we recall the standard definitions and physical meaning of the two most popular measures of two-qubit entanglement, i.e., the negativity and concurrence, which are in the following sections compared with the measures of steering and Bell nonlocality.

The negativity is defined as $N(\rho) = \max\{0, -2\mu_{\min}\}$, where $\mu_{\min} = \min \text{eig}(\rho^\Gamma)$ and ρ^Γ denotes a partial transpose of ρ . It was first introduced in Ref. [51] as a quantitative version of the Peres-Horodecki entanglement criterion [52]. The two-qubit negativity (or, more directly, the logarithmic negativity $\log_2[N(\rho) + 1]$) has various quantum-information interpretations. Specifically, (i) it is a measure of the entanglement cost under operations preserving the positivity of the partial transpose for two-qubit systems [53,54], (ii) it gives an upper bound of distillable entanglement [5], and (iii) it determines the dimensionality of entanglement, i.e., the number of the degrees of freedom of entangled subsystems [55].

The Wootters concurrence [56], which is monotonically related to the entanglement of formation, is given by $C(\rho) = \max\{0, 2\lambda_{\max} - \sum_j \lambda_j\}$, where $\lambda_j^2 = \text{eig}[\rho(\sigma_2 \otimes \sigma_2)\rho^*(\sigma_2 \otimes \sigma_2)]_j$, with σ_2 denoting the Pauli Y operator, and $\lambda_{\max} = \max_j \lambda_j$. Note that both measures have been applied in quantifying not only entanglement but also, e.g., nonclassicality (quantumness) of single-qubit (or single-qudit) states [57–59]. These two related measures reach unity for the Bell states and vanish for separable states. For the brevity of our presentation, we have plotted the negativity as the only entanglement measure.

These entanglement measures of various two-qubit states have been typically determined experimentally only indirectly, based on a full QST, which is also the case in this work. Note that an experimental universal test of entanglement without a complete QST was proposed in Ref. [60] (see Appendix A). This test is a necessary and sufficient criterion of two-photon polarization entanglement. It is based on measuring a collective universal witness of Ref. [61], which gives tight lower and upper bounds for the negativity and concurrence, and can be used as an entanglement measure on its own. However, since its quantum-information interpretation and applications are limited, we prefer to use the standard entanglement measures, even if they are determined indirectly using experimental density matrices.

B. Steerable weight

The steerable weight [62] and the steering robustness [63] are arguably the most popular measures of EPR steering [7,8,64]. They can be applied for quantifying not only standard spatial steering, but also (after a minor modification) to quantify temporal [13,16,17,65,66] and spatiotemporal [67] steering.

An intuitive and general idea behind the steerable weight, according to Skrzypczyk *et al.* [62], is based on the decomposition of a given assemblage of Alice, $\sigma_{a|x}$, into its steerable ($\sigma_{a|x}^s$) and unsteerable ($\sigma_{a|x}^{\text{us}}$) parts, for the values of a and x specified in Appendices B and C, i.e.,

$$\sigma_{a|x} = \mu \sigma_{a|x}^{\text{us}} + (1 - \mu) \sigma_{a|x}^s \quad (2)$$

for $\mu \in [0, 1]$. Note that the unsteerable assemblages $\sigma_{a|x}^{\text{us}}$ can be created via classical strategies, and a model based on $\sigma_{a|x}^{\text{us}}$ can be referred to as an LHS model. The steerable weight $S = 1 - \mu^*$ is defined as the maximum amount of unsteerable assemblage $\sigma_{a|x}^{\text{us}}$ necessary to reproduce Alice's assemblage $\sigma_{a|x}$. This general definition can be formulated as solutions of semidefinite programs (SDPs) as demonstrated in Refs. [7,62] and are given explicitly in Appendices B and C for the 3MS and 2MS, respectively. Moreover, sufficient and necessary conditions for observing steering in multimeasurement scenarios are discussed in Appendix D.

The LHS models are relevant to quantum steering as follows [10]: A given state ρ is referred to as quantum (EPR) unsteerable (in the communication from Alice to Bob) for Alice's measurement set $\{M_{a|x}\}$ if one can find a variable λ allowing for the Bell local decomposition [7,8]

$$p(ab|xy) = \int d\lambda \pi(\lambda) p_A(a|x, \lambda) \text{Tr}(M_{b|y} \sigma_\lambda), \quad (3)$$

where σ_λ is the local (hidden) quantum state of Bob and $p_A(a|x, \lambda)$ is Alice's response distribution. Otherwise a given state for the measurement set $\{M_{a|x}\}$ is referred to as quantum (EPR) steerable, i.e., when its statistics cannot be reproduced by an LHS model. Note that Eq. (7), which defines a Bell local state, reduces in the special case to Eq. (3) by setting $p_B(b|y, \lambda) = \text{Tr}(M_{b|y} \sigma_\lambda)$. It is usually assumed that Bob's measurements $M_{b|y}$ enable a complete QST of his qubit. The collection of Bob states $\sigma_{a|x} = \text{Tr}_A(M_{a|x} \otimes \mathbb{1} \rho)$, conditioned on Alice's measurements, is called an assemblage.

The steerable weight and, equivalently, the steering robustness of Ref. [63] are defined via necessary and sufficient conditions for quantum-information characterization of quantum steering in the specified measurement scenarios. Thus, a spatially separated two-qubit state ρ is referred to as steerable (or more precisely S_n steerable) in the discussed n -measurement scenarios if there exists a set of measurements such that the steerable weight is nonvanishing, $S_n(\rho) > 0$. Otherwise it is referred to as unsteerable (or S_n unsteerable).

The question arises why our interest is focused on analyzing steering in two- and three- measurement scenarios only, except in Sec. VIC and Appendix D. In principle, one could also consider steering in the limit of an infinite number (of the types) of measurements, but this would require knowing universal criteria (i.e., which are both sufficient and necessary) for detecting this type of steering. Unfortunately, such universal criteria are not known for the GWSs. Note that the upper and lower bounds for steering have only been calculated numerically so far for large but still finite numbers n of measurements [i.e., at most for $n = 136$, as shown in Fig. 8(a) based on the results of Refs. [68,69]]. Moreover, our analysis of steering includes not only criteria but also steering measures, as shown in Figs. 2–5. Unfortunately, the calculations of the steerable weight and the steering robustness are much more involved beyond 3MS. Finally, we remark that our experimentally generated states are not exactly GWSs, so the calculations of their measures or even universal criteria of steering beyond the 3MS are even more complicated compared to those for the perfect GWSs.

C. Horodecki measure of Bell nonlocality

Here we recall the Horodecki measure [70,71] of quantum nonlocality for two-qubit states. Note that quantum nonlocality is usually studied and interpreted in the context of Bell inequalities (including the CHSH inequality) and then it is often referred to as Bell(-CHSH) nonlocality [6]. A Bell inequality violation (BIV) demonstrates the impossibility of any LHV models to fully reproduce quantum-mechanical predictions [4]. For convenience, we use the terms BIV and Bell(-CHSH) nonlocality interchangeably, in the context of our two-qubit experiments. Note that BIV implies a violation of local realism. So BIV can in principle be explained by *nonlocal* (non)realistic theories, but also by *local* nonrealistic ones. Moreover, quantum nonlocality can be defined without referring to BIV. In addition, such (generalized) quantum nonlocality can occur without quantum entanglement in, e.g., three qubits or two qutrits (three-level systems) [72]. Thus, it should be stressed that, in general, BIV does not imply quantum nonlocality nor does quantum nonlocality imply BIV (see, e.g., Refs. [6,73]).

The Horodecki measure of Bell nonlocality for a two-qubit state ρ quantifies the amount of the maximal violation of the Bell-CHSH inequality [9],

$$|\langle \mathcal{B} \rangle| = |\mathcal{E}(\phi_1, \phi_2) + \mathcal{E}(\phi'_1, \phi_2) + \mathcal{E}(\phi_1, \phi'_2) - \mathcal{E}(\phi'_1, \phi'_2)| \leq 2, \quad (4)$$

which is given in terms of the Bell-CHSH operator $\mathcal{B} = \mathbf{a} \cdot \boldsymbol{\sigma} \otimes (\mathbf{b} + \mathbf{b}') \cdot \boldsymbol{\sigma} + \mathbf{a}' \cdot \boldsymbol{\sigma} \otimes (\mathbf{b} - \mathbf{b}') \cdot \boldsymbol{\sigma}$. Moreover, ϕ_i and ϕ'_i are two dichotomic variables of the i th ($i = 1, 2$) qubit

corresponding to the rotations of a polarizer in typical optical implementations, while $\mathcal{E}(\phi_1, \phi_2)$ is the expectation value of the joint measurement of ϕ_1 and ϕ_2 , and analogously for the other expectation values. For a given two-qubit state ρ , the expected value of the Bell-CHSH operator \mathcal{B} , which is maximized over real-valued three-dimensional unit vectors \mathbf{a} , \mathbf{a}' , \mathbf{b} , and \mathbf{b}' , reads [70,71]

$$\max_{\mathcal{B}} \text{Tr}(\rho \mathcal{B}_{\text{CHSH}}) = 2\sqrt{M(\rho)}, \quad (5)$$

where $M(\rho) = \max_{j < k} \{h_j + h_k\} \leq 2$, and h_j ($j = 1, 2, 3$) are the eigenvalues of $U = T^T T$, which is the real symmetric matrix constructed from the correlation matrix T (and its transpose T^T) defined below Eq. (1). Thus, the Bell-CHSH inequality is violated if $M(\rho) > 1$ [70,71]. To quantify the degree of BIV and Bell nonlocality we apply the parameter [74]

$$B(\rho) \equiv \sqrt{\max[0, M(\rho) - 1]}. \quad (6)$$

Note that this nonlocality measure is exactly equal to the concurrence and negativity for two-qubit *pure* states. For a given state ρ , the Bell-CHSH inequality in Eq. (4) is satisfied if and only if $B(\rho) = 0$. If $B(\rho) = 1$ then the inequality is maximally violated, which is the case for Bell states. We refer to $B(\rho)$ as a Bell nonlocality measure.

In this work we refer to Bell nonlocal and local states with the following meaning. Usually, a spatially separated state is referred to as Bell local if local measurements and classical communication can generate a correlation admitting an LHV model [4,6]. Otherwise the state is referred to as Bell nonlocal.

More specifically, an LHS model can be introduced by considering two distant observers (Alice and Bob) who share an entangled two-qubit state ρ . Assume that Alice (Bob) performs a set of measurements $\{M_{a|x}\}$ ($\{M_{b|y}\}$) satisfying $M_{a|x}, M_{b|y} \geq 0$ and $\sum_a M_{a|x} = \sum_b M_{b|y} = \mathbb{1}$, where x and y label measurements and a and b are their outcomes. The resulting statistics $p(ab|xy) = \text{Tr}(M_{a|x} \otimes M_{b|y} \rho)$ are referred to as Bell local (with respect to the measurement sets $\{M_{a|x}\}$ and $\{M_{b|y}\}$) if they allow for a Bell local decomposition [6]

$$p(ab|xy) = \int d\lambda \pi(\lambda) p_A(a|x, \lambda) p_B(b|y, \lambda), \quad (7)$$

where λ is a shared local hidden variable distributed with density $\pi(\lambda)$, while $p_A(a|x, \lambda)$ and $p_B(b|y, \lambda)$ are local response distributions. Thus, a state is called Bell local if it can be reproduced by an LHV model with properly chosen $\{\lambda, \pi(\lambda), p_A(a|x, \lambda), p_B(b|y, \lambda)\}$. Otherwise the state is referred to as Bell nonlocal for the measurement sets $\{M_{a|x}\}$ and $\{M_{b|y}\}$. This Bell nonlocality can be witnessed by the violation of a Bell inequality, which reduces to testing the Bell-CHSH inequality in the case of two-qubit states. So, in terms of the Horodecki measure, a given two-qubit state is Bell local (nonlocal) if and only if $B(\rho) = 0$ [$B(\rho) > 0$].

The Horodecki measure of Bell nonlocality can be determined without a complete QST, which was experimentally demonstrated in an entanglement-swapping device in [75] (see Appendix A). However, here we apply a full QST for determining ρ_{GW}^E and then calculating $B(\rho_{\text{GW}}^E)$.

Note that various alternative approaches to quantifying nonlocality have been proposed [6]. These include a nonlocal-

ity measure introduced by Elitzur *et al.* in Ref. [76], which can be interpreted as a fraction of a given ensemble that cannot be expressed via local correlations. Thus, this quantifier has been referred to as a fraction of nonlocality [77,78].

IV. GENERALIZED WERNER STATES AND THEIR EXPERIMENTAL GENERATION

In this work we focus on comparing quantum correlations of experimental states, which are special cases of those in Eq. (1). Specifically, we directly generate Werner(-like) states (also referred to as isotropic states or Bell states with white noise) [11]

$$\rho_W = p|\phi^+\rangle\langle\phi^+| + \frac{1-p}{4}I \otimes I, \quad (8)$$

which are mixtures of any Bell state [say, $|\phi^+\rangle = (|00\rangle + |11\rangle)/\sqrt{2}$] and the maximally mixed state for various values of the mixing parameter $p \in [0, 1]$. Note that the original definition of the Werner state is based on the singlet state [11], instead of $|\phi^+\rangle$. However, this local change does not effect measures of entanglement, steering, and nonlocality. Thus, the state defined in Eq. (8) is also often referred to as a Werner state (see, e.g., Refs. [35,69,74,79,80]). This terminology is used in this paper.

We are also interested in partially entangled states with white noise, which we call GWSs, which are obtained from Eq. (8) by replacing $|\phi^+\rangle$ by a general two-qubit pure state $|\phi_q\rangle = \sqrt{q}|00\rangle + \sqrt{1-q}|11\rangle$ with the superposition coefficient $q \in [0, 1]$. Thus, the GWSs can be defined as

$$\rho_{GW}(p, q) = p|\phi_q\rangle\langle\phi_q| + \frac{1-p}{4}I \otimes I. \quad (9)$$

These states for $q = \frac{1}{2}$ can be referred to as the Bell-diagonal GWSs corresponding to the Werner states $\rho_W(p)$, which are diagonal in the Bell basis, while for $q \neq \frac{1}{2}$ we refer to them as the Bell-nondiagonal GWSs. These states have been generated by us in the experimental setup described below.

Experimental setup

Here we describe our experimental setup, which is designed to be as versatile as possible, being capable of generating a broad class of mixed quantum states in the form

$$\rho = \begin{pmatrix} A & 0 & 0 & E \\ 0 & B & F & 0 \\ 0 & F^* & C & 0 \\ E^* & 0 & 0 & D \end{pmatrix}. \quad (10)$$

This class of states includes (i) the Werner [11] and Werner-like states, (ii) the Horodecki states, which are mixtures of a Bell state and a separable state orthogonal to it [52], (iii) Bell-diagonal states (including the Werner states), and (iv) various types of MEMSs, e.g., those defined in [35]. Moreover, the capabilities of our method are not limited to the Werner or Horodecki states based on a ‘‘balanced’’ Bell state, but also allow for (v) their generalized forms based on unbalanced entangled states $\sqrt{1-q}|00\rangle + \sqrt{q}|11\rangle$ for any $q \in [0, 1]$ instead of considering only $q = \frac{1}{2}$.

In this work we focus on experimentally generating the Werner states and GWSs, which are prepared on a platform of

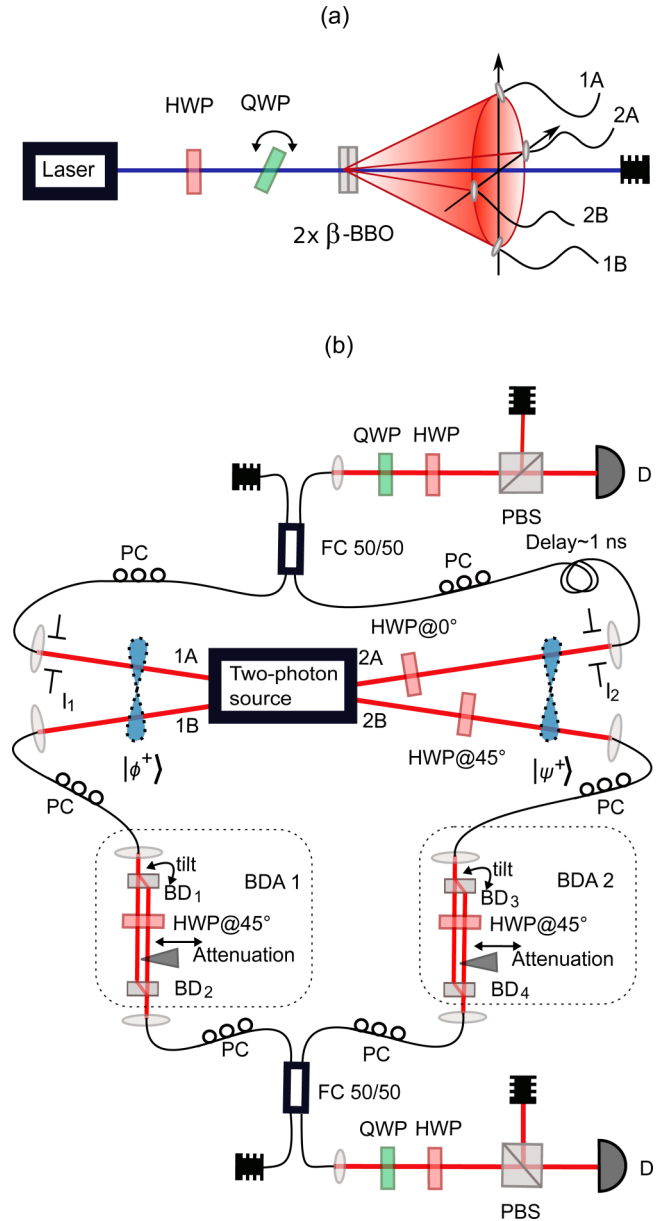


FIG. 1. Our experimental setups for (a) photon-pair generation and (b) state synthesis: 1A and 1B (2A and 2B), photons propagating in vertical (horizontal) planes; BD, beam displacer; BDA, beam displacer assembly; D, detector; FC, fiber coupler; HWP, half waveplate; PBS, polarization beam splitter; PC, polarization controller; QWP, quarter waveplate; I₁ and I₂, irises 1 and 2; and β-BBO, β barium borate (a nonlinear crystal).

quantum linear optics using the experimental setup depicted in Fig. 1. Qubits are encoded into polarization states of single photons. The process of type-I SPDC occurring in a cascade of two nonlinear β-BBO crystals serves as a source of entangled photons [81]. When pumped by a beam at a wavelength of $\lambda = 355$ nm, the source generates two polarization-entangled photons in mutually different spatial modes at $\lambda = 710$ nm [Fig. 1(a)]. The state of these photons can be expressed in the form $|\phi^+\rangle = (|00\rangle + |11\rangle)/\sqrt{2}$, where $|0\rangle$ and $|1\rangle$ denote horizontally (H) and vertically (V) polarized photons, respectively. Due to the geometry of type-I SPDC, photons are

generated in symmetrically opposite directions on the surface of a cone with its axis coincidental with the pump beam. We choose to couple photon pairs propagating in the vertical and horizontal planes, denoting them by (1A,1B) and (2A,2B), respectively [see Fig. 1(a)]. Assuming that only two photons were generated (so higher-photon-number processes are negligible), these photons are simultaneously in either modes (1A,1B) or (2A,2B). Employing a half-wave plate (HWP) at 45° in the 2B mode, the state $|\phi^+\rangle$ is transformed into the Bell state $|\psi^+\rangle = (|01\rangle + |10\rangle)/\sqrt{2}$. Thus, we obtain states spanning the two subspaces $|\phi^+\rangle$ and $|\psi^+\rangle$.

Our goal is to prepare the Werner states and their generalizations for various values of the mixing parameter p . The main idea behind the design of our setup is to decrease temporal coherence of the states $|\phi^+\rangle$ (in the modes 1A and 1B) and $|\psi^+\rangle$ (in the modes 2A and 2B) using beam displacer assemblies (BDAs). A BDA consists of a pair of beam displacers (BDs) with an HWP inserted between them. This allows us to split and subsequently rejoin the horizontal and vertical components of a photon polarization state. By introducing a difference in the propagation time between these two components (which is done by tilting one BD) we can achieve their mutual phase difference (by fine tilting) and tunable distinguishability (by coarse tilting). Polarization-sensitive losses can easily be implemented by partially blocking one of the polarization paths. Subsequently, the modes (1A,2A) and (1B,2B) are incoherently mixed in fiber couplers.

First, the subspace $|\phi^+\rangle$ is adjusted while arms 2A and 2B (belonging to the subspace $|\psi^+\rangle$) are blocked. By means of the polarization-sensitive losses in BDA_1 , we regulate the intensity ratio of the matrix elements A and D [see Eq. (10)] in the computational basis, i.e., $|00\rangle$ and $|11\rangle$ (or $|HH\rangle$ and $|VV\rangle$ in the polarization terms). The ratio accounts for

$$R_{A,D} = \frac{4pq + 1 - p}{4p(1 - q) + 1 - p}, \quad (11)$$

where p and q are both tuned parameters. The next step consists of tuning the decoherence by observing coincidence counts in the projections $|++\rangle$ and $|+-\rangle$, where $|\pm\rangle = (|0\rangle \pm |1\rangle)/\sqrt{2}$ stand for diagonal and antidiagonal polarization states, respectively. We find such a coarse tilt of BD_1 so that the visibility accounts for

$$v = \frac{2E}{A + D}, \quad (12)$$

while the phase is set by fine-tuning the tilt using a piezoactuator, which minimizes the signal in the $|+-\rangle$ projection by setting the effective value of E to be real.

Second, when adjusting the subspace $|\psi^+\rangle$ in turn, the arms 1A and 1B are blocked. In analogy with the adjustment of the $|\phi^+\rangle$ subspace, the same two steps are performed. This time, however, the target intensity ratio $R_{B,C}$ is equal to 1 because $B = C$. The coarse tilt of BD_3 needs to be sufficient to decrease the coherence of the state completely since $v = 0$, resulting in $F = 0$. The phase becomes meaningless.

Finally, all arms are unblocked and both subspaces are balanced to adjust the ratio between the matrix elements A and B . While having the projection of $|00\rangle$ and $|01\rangle$, the required

ratio is

$$R_{A,B} = \frac{4pq + 1 - p}{1 - p}. \quad (13)$$

For this purpose, we partially close the irises in the 1A and 2A couplers, which are depicted in Fig. 1(b) by labels I_1 and I_2 , respectively.

After all the adjustments are implemented, the measurement itself is carried out and it consists of a standard full QST [82]. Polarization projection is performed on both photons utilizing a set of quarter and half waveplates, as well as polarizers and single-photon detectors. Coincidence detections within a 2-ns window are detected under all 36 twofold combinations of single-photon projections onto the basis states $|0\rangle$, $|1\rangle$, $|+\rangle$, $|-\rangle$, and $(|0\rangle \pm i|1\rangle)/\sqrt{2}$, where the latter states are the right- and left-hand circularly polarized states, respectively. Density matrices are estimated via a maximum-likelihood method [83–87].

Because of experimental imperfections, the setup produces states with the p and q parameters slightly different from those targeted by the above-described procedure. To observe better agreement with theoretical predictions, we estimate the best-fitting parameters p_{est} and q_{est} by finding such a $\rho_{\text{GW}}(p_{\text{est}}, q_{\text{est}})$ that its fidelity with the experimentally reconstructed density matrix is maximized. We find that the deviations of the estimated value of the mixing parameter p_{est} from the value of p , which is set with a limit precision in our experiment, are on average equal to 0.01 for the Werner states and 0.03 for the GWSs. For the estimated value of the superposition parameter q_{est} , the observed parameter deviations from a given value of q are equal on average to 0.02. The maximal deviation values are 0.03 for both Werner states and GWSs. Note that the superposition parameter q is manually set by an HWP in the source part of the setup shown in Fig. 1(a). Experimental data as well as the estimated density matrices are provided in the Supplemental Material [88].

The states ρ_{W} and ρ_{GW} can also be expressed by Eq. (10) with $F = 0$. In this matrix, the subspace spanned by the states $|\phi_q\rangle$ for $q \in [0, 1]$ is represented by the elements A , D , E , and E^* , while the corresponding subspace for the white-noise term corresponds to only diagonal elements (A , B , C , D). For the reasons specified below, we set, in our experiments, the superposition coefficient at $q = 0.9$, in addition to $q = 0.5$.

Note that it is irrelevant to replace $|\phi_q\rangle$ by a four-term superposition state $|\phi_{abcd}\rangle = a|00\rangle + b|01\rangle + c|10\rangle + d|11\rangle$ at least in the analysis of nonclassical correlations. This is because $|\phi_{abcd}\rangle$ can be reduced to $|\phi_q\rangle$ solely by local rotations, so the studied two-qubit quantum correlations are unchanged. As mentioned above, the GWSs are not diagonal in the Bell basis, except $q = 0, \frac{1}{2}, 1$. This property greatly complicates analytical calculations of correlation measures. So, for the Bell-nondiagonal GWSs, we present analytical formulas of the entanglement and nonlocality measures only, contrary to the corresponding results for the Werner states, which include also our formulas for the steerable weights.

We begin our detailed comparative analysis by presenting various theoretical relations between chosen correlation measures for the Werner states and GWSs showed in Figs. 2 and 3, respectively. These curves show the negativity N (or equivalently the concurrence C), the steerable weights S_2 and S_3 ,

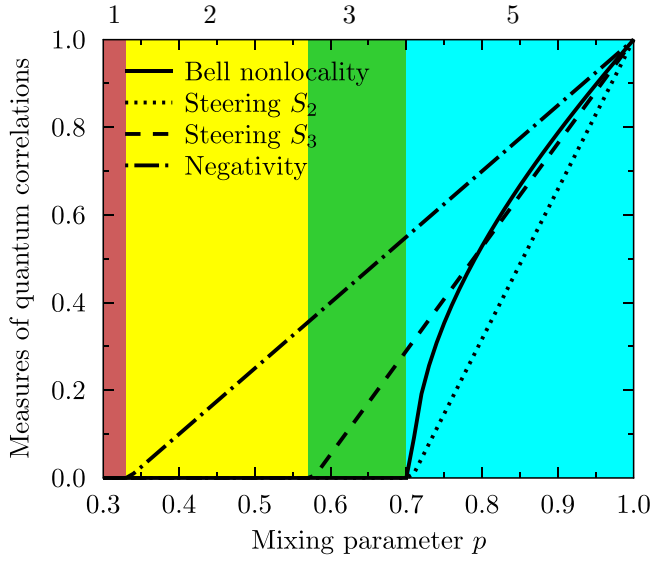


FIG. 2. Four correlation regimes of the Werner states corresponding to those listed in Table I. Note that regime 4 is missing. Theoretical plots for the negativity N (or, equivalently, the concurrence C), the steerable weights S_2 and S_3 , and the Bell nonlocality measure B are shown as a function of the mixing parameter p . Exact definitions of the depicted quantum correlation measures are given in Sec. V.

and the Bell nonlocality measure B as a function of the mixing parameter p . Each colored region starts where a given correlation measure becomes nonzero with an increasing value of the mixing parameter p . We refer to these regions as quantum correlation regimes, which are also listed in Tables I and II.

V. HIERARCHY OF THE CLASSES OF CORRELATIONS FOR WERNER-LIKE STATES

A. Entanglement of Werner-like states

It is well known that, for Werner states, the concurrence and negativity, which were defined in Sec. III A, are equal to each other and are given by a linear function of the mixing parameter p , i.e.,

$$N(\rho_W) = C(\rho_W) = \max[0, (3p - 1)/2], \quad (14)$$

as shown in Fig. 2 by the dot-dashed curve. The good agreement of the negativities calculated for the theoretical and experimental Werner states is shown in Fig. 4(a).

We find that the negativity and concurrence for the GWSs read

$$N(\rho_{GW}) = C(\rho_{GW}) = \max\left\{0, \frac{1}{2}[p(1 + 4\sqrt{x}) - 1]\right\}, \quad (15)$$

with $x = q(1 - q)$, which is plotted in Fig. 3 by the dot-dashed curve. Figure 5(a) demonstrates the good fit of the negativities calculated for the theoretical and experimental GWSs for different values of the superposition parameter q . Note that not only $N(\rho_W)$ but also $N(\rho_{GW})$ is a linear function of the mixing parameter p for a fixed value of the superposition coefficient q . In a special case for a pure state $|\phi_q\rangle$ (i.e., when $p = 1$), Eq. (15) reduces to $N(|\phi_q\rangle) = C(|\phi_q\rangle) = 2\sqrt{q(1 - q)}$.

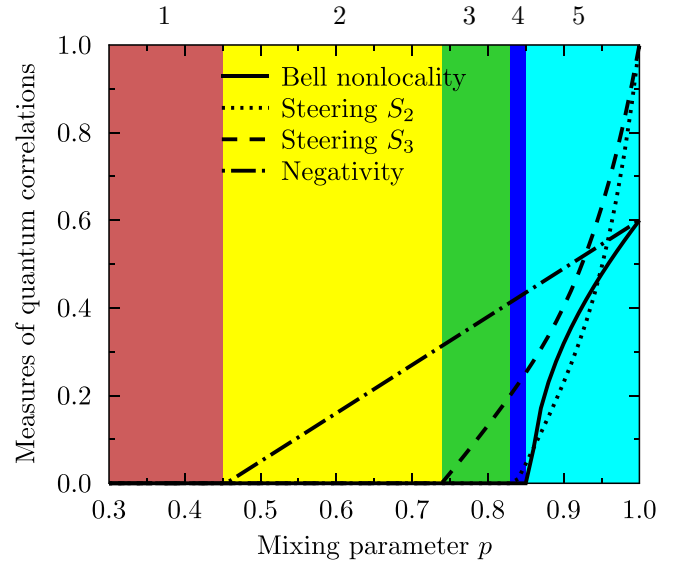


FIG. 3. Five correlation regimes of the GWSs corresponding to the regimes in Table II. Curves are analogous to those in Fig. 2, but for the superposition parameter $q = 0.9$ or, equivalently, $q = 0.1$.

Equation (15) vanishes for $p \in [0, p_N(q)]$ at the threshold value given by

$$p_N(q) = 1/[1 + 4\sqrt{q(1 - q)}], \quad (16)$$

which is plotted in Fig. 6. It can be seen that $N[\rho_W(p)] > 0$ if $p > \frac{1}{3}$ and $N[\rho_{GW}(p, 0.9)] > 0$ if $p > p'_N = \frac{5}{11}$. These threshold values are below those for the other measures of quantum correlations and also marked in Figs. 6 and 7.

Note that $N(\rho_{GW}) = C(\rho_{GW})$ should hold for the ideal GWSs, including the Werner states. However, our experimental GWSs do not exactly satisfy this condition. Thus, we calculate both measures, because their difference shows how much our experimental states deviate from the ideal Werner states. These deviations quantify also the precision of our measurements. Specifically, the observed experimental differences between the negativity and concurrence are on the average 0.02% for the Werner states and 0.06% for the GWSs. Thus, on the scale of Figs. 4(a) and 5(a) one could not see any differences between $N(\rho_{GW}^E)$ and $C(\rho_{GW}^E)$.

B. Steering of Werner-like states in the three-measurement scenario

Steering in a 3MS on Alice's side can be quantified by the steerable weight S_3 of Ref. [62], as defined as an SDP in Appendix B. We find that this steerable weight S_3 for the Werner states is a *linear* function of the mixing parameter p , specifically,

$$S_3(\rho_W) = \max\left(0, \frac{\sqrt{3}p - 1}{\sqrt{3} - 1}\right), \quad (17)$$

which means that the state $\rho_W(p)$ is steerable in the 3MS if $p > 1/\sqrt{3}$ [see Fig. 4(d) and Table I]. By contrast, the steerable weight S_3 for the GWSs is a *nonlinear* function of the mixing parameter p for $q \neq \frac{1}{2}$. This is shown for $q = 0.9$ in Fig. 5(d). It can be seen that these GWSs are steerable for $p >$

TABLE I. Hierarchy of classes of correlations for the Werner states $\rho_W(p)$ depending on the mixing parameter p . The four regimes of vanishing or nonvanishing different classes of quantum correlations correspond to the regimes shown in Figs. 2 and 4.

Regime	B	$S_2 \equiv S_2^{ij}$	S_3	N	p	Expt.
1	$B = 0$	$S_2 = 0$	$S_3 = 0$	$N = 0$	$p \in [0, \frac{1}{3}]$	direct
2	$B = 0$	$S_2 = 0$	$S_3 = 0$	$N > 0$	$p \in (\frac{1}{3}, \frac{1}{\sqrt{3}}]$	direct
3	$B = 0$	$S_2 = 0$	$S_3 > 0$	$N > 0$	$p \in (\frac{1}{\sqrt{3}}, \frac{1}{\sqrt{2}}]$	direct
4	$B = 0$	$S_2 > 0$	$S_3 > 0$	$N > 0$	$p \in \emptyset$	impossible
5	$B > 0$	$S_2 > 0$	$S_3 > 0$	$N > 0$	$p \in (\frac{1}{\sqrt{2}}, 1]$	direct

$p_{S_3} = 0.7390$ (see also Table II). This means that $\rho_{GW}(p, 0.9)$ is steerable for a much shorter range of the mixing parameter p than that for $\rho_W(p) \equiv \rho_{GW}(p, \frac{1}{2})$. Figures 4(d) and 5(d) show the weight S_3 for our experimental states compared to those for the theoretical states. These results show good agreement of the theory with our experimental results.

C. Steering of Werner-like states in two-measurement scenarios

To quantify steering of the Werner states and GWSs in 2MSs on the Alice side, we apply the steerable weights S_2^{ij} of Ref. [62] defined in Appendix C. We find that the weights S_2^{ij} for the Werner states are equal to each other, $S_2(\rho_W) \equiv S_2^{XY}(\rho_W) = S_2^{XZ}(\rho_W) = S_2^{YZ}(\rho_W)$, being a linear function of the mixing parameter p , i.e.,

$$S_2(\rho_W) = \max\left(0, \frac{\sqrt{2}p - 1}{\sqrt{2} - 1}\right). \tag{18}$$

This implies the steerability of the states in the 2MS if $p > 1/\sqrt{2}$ [see Fig. 4(c) and Table I]. However, the steerable weights for the GWSs become much more complicated. We find that $S_2^{XY}(\rho_{GW}) \leq S_2^{XZ}(\rho_{GW}) = S_2^{YZ}(\rho_{GW}) \equiv S_2(\rho_{GW})$ and there exist two threshold values p'_{S_2} and p'_B , as listed in Table II. Specifically, (i) $S_2^{XZ}(\rho_{GW}) = S_2^{YZ}(\rho_{GW}) > 0$ if $p > p'_{S_2} = 0.8370\dots$ and (ii) $S_2^{XY}(\rho_{GW}) > 0$ if $p > p'_B = 5/\sqrt{32}$, which is the same threshold parameter as that for the Bell nonlocality measure $B > 0$, as discussed above. Moreover, the dependence of $S_2^{ij}(\rho_{GW})$ on the mixing parameter p becomes nonlinear for $q \neq \frac{1}{2}$. Different values of the threshold parameters for p'_B and p'_{S_2} imply the occurrence of region 4 for the

GWSs, which is shown in Figs. 3, 6(a), and 7(c) and explained in detail in Sec. VI A.

D. Nonlocality of Werner-like states

To estimate the degree of quantum nonlocality or, equivalently, to quantify the violation of the Bell-CHSH inequality for two-qubit states [9], we use the Horodecki measure [70,71], which is as defined in Sec. III C. The Bell nonlocality measure for the Werner states reads

$$B(\rho_W) = \sqrt{\max(0, 2p^2 - 1)}, \tag{19}$$

which instantly implies a standard result that the Werner states are nonlocal if $p > 1/\sqrt{2}$ (see also Table I). However, if $p \in (\frac{1}{3}, 1/\sqrt{2})$, the Werner states are entangled without BIV (admitting an LHV model), as already demonstrated by Werner in [11].

We find that the Bell nonlocality measure for the GWSs is given by

$$B(\rho_{GW}) = \max\{0, \sqrt{p^2[1 + 4q(1 - q)] - 1}\}. \tag{20}$$

Note that for pure states ($p = 1$), Eq. (20) reduces to the standard result $B(|\phi_q\rangle) = N(|\phi_q\rangle) = 2\sqrt{q(1 - q)}$. It can be seen that $B(\rho_{GW})$ is zero for the values of the mixing parameter in the range $p \in [0, p_B(q)]$ with the threshold value given by

$$p_B(q) = 1/\sqrt{1 + 4q(1 - q)}, \tag{21}$$

which is plotted in Fig. 6. For the diagonal GWSs (with $q = \frac{1}{2}$), we can reproduce the well-known threshold value $p_B(\frac{1}{2}) = 1/\sqrt{2}$ for the Werner states. In another special case for $q = 0.9$, which was set in our experiments, we have the

TABLE II. Hierarchy of classes of correlations exhibited by the Bell-nondiagonal GWSs $\rho_{GW}(p, q)$ for different values of the mixing parameter p and a fixed value of the superposition parameter at $q = 0.9$ or, equivalently, $q = 0.1$. This table lists the five regimes shown in Figs. 3, 5, and 6(a). The threshold values read $p'_N \equiv p_N(q) = \frac{5}{11} = 0.45(45)$ and $p'_B \equiv p_B(q) = 5/\sqrt{32} = 0.8574\dots$, as given by Eqs. (16) and (21) for $q = 0.9$ (or 0.1), respectively, while $p'_{S_3} \equiv p_{S_3}(q) = 0.7390\dots$ and $p'_{S_2} \equiv p_{S_2}(q) = 0.8370\dots$ were obtained numerically. The term *hybrid* experiment refers to averaging of two directly generated experimental states according to Eq. (23). Here 2MS and 3MS stand for two- and three-measurement scenarios, respectively.

Regime	States	B	S_2^{XY}	$S_2 \equiv S_2^{XZ} = S_2^{YZ}$	S_3	N	p	Expt.
1	separable	$B = 0$	$S_2^{XY} = 0$	$S_2 = 0$	$S_3 = 0$	$N = 0$	$p \in [0, p'_N]$	direct
2	3MS unsteerable but entangled	$B = 0$	$S_2^{XY} = 0$	$S_2 = 0$	$S_3 = 0$	$N > 0$	$p \in (p'_N, p'_{S_3}]$	direct
3	steerable in 3MS but not in 2MS	$B = 0$	$S_2^{XY} = 0$	$S_2 = 0$	$S_3 > 0$	$N > 0$	$p \in (p'_{S_3}, p'_{S_2}]$	direct
4	Bell local but 2MS steerable	$B = 0$	$S_2^{XY} = 0$	$S_2 > 0$	$S_3 > 0$	$N > 0$	$p \in (p'_{S_2}, p'_B]$	hybrid
5	Bell nonlocal	$B > 0$	$S_2^{XY} > 0$	$S_2 > 0$	$S_3 > 0$	$N > 0$	$p \in (p'_B, 1]$	direct

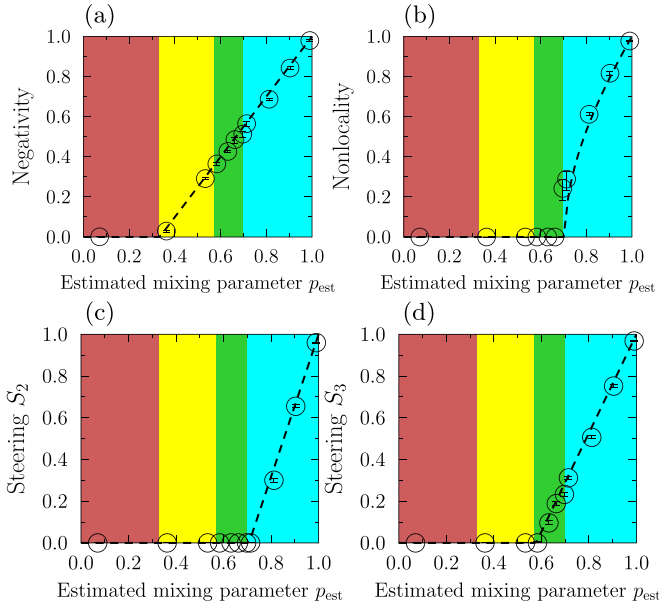


FIG. 4. Quantum correlations for the theoretical and experimental Werner states as a function of the estimated mixing parameter p_{est} : (a) negativity N , (b) Bell nonlocality measure B , and steerable weights (c) S_2 and (d) S_3 .

threshold value $p'_B \equiv p_B(q = 0.9) = p_B(q = 0.1) = 5/\sqrt{32}$. Thus, the GWSs $\rho_{\text{GW}}(p, 0.9)$ for $p \in (p'_N, p'_B) = (\frac{5}{11}, 5/\sqrt{32})$ are entangled without Bell nonlocality, which occurs for a wider range of the mixing parameter p compared to that for the Werner states, i.e., $p'_B - p'_N \approx 0.4029 > 1/\sqrt{2} - \frac{1}{3} \approx 0.3738$, as it is explained in detail in Sec. VI B.

In Fig. 4(b) we plot $B(\rho_W)$ in comparison to the numerically calculated $B(\rho_W^E)$ for the experimental Werner states $\rho_W^E(p)$ for various values of the mixing parameter p and fixed $q = 0.9$. Analogous results for the Bell nonlocality measure $B(\rho_{\text{GW}})$ for the GWSs generated experimentally, $\rho_{\text{GW}}^E(p; q = 0.9)$, are shown in Fig. 5(b) in comparison to those for the ideal GWSs, $\rho_{\text{GW}}(p; q = 0.9)$. Note that $B(\rho_{\text{GW}}) > 0$ if $p > p'_B$ (see also Table II), assuming $q = 0.9$ or 0.1 , which is clearly larger than the corresponding threshold value $1/\sqrt{2}$ for the Werner states. Both Figs. 4(b) and 5(b) show relatively good agreement of our experimental results compared to the corresponding theoretical predictions. More details about the accuracy of our experimental results were given in Sec. IV.

VI. COUNTERINTUITIVE RESULTS

Here we present the, arguably, most interesting theoretical results of our paper for the states generated experimentally (either directly or in a hybrid way).

A. Steerability S_2 without Bell nonlocality

Here we show that Bell-nondiagonal GWSs are steerable in 2MSs on Alice's side but still admit an LHV model. So the existence of such quantum correlations cannot be revealed by the violation of the Bell-CHSH inequality. The GWSs exhibiting the S_2 steerability without Bell nonlocality correspond to regime 4 in Table II and are shown in Figs. 3, 6(a), and 7(c).

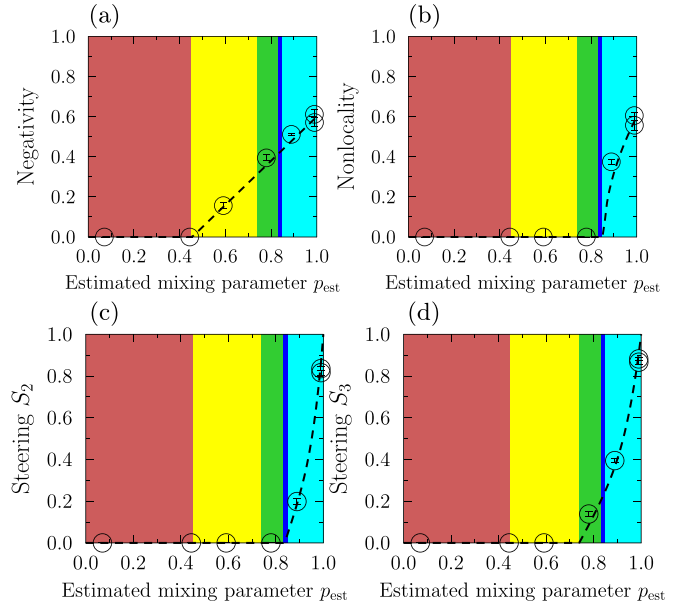


FIG. 5. Same as in Fig. 4 but for the GWSs for the estimated superposition coefficient $q_{\text{est}} \approx q = 0.9$ (see the text for details).

Our analytical and numerical results clearly demonstrate that regime 4 cannot be observed for the Werner states, for which $p_B(\frac{1}{2}) = p_{S_2}(\frac{1}{2})$ holds, as can be seen in Fig. 2. However, this degeneracy is broken for the GWSs with $q \neq 0, \frac{1}{2}, 1$. We find this result interesting, although the amount of the required white noise destroying the correlations is small [i.e., $\max_q \Delta_{B, S_2}(q) = 0.023$] compared to all the other cases shown in Fig. 7, except Fig. 7(e).

Moreover, regime 4 can be observed for the mixing parameter p limited to a very narrow range $[p'_{S_2}, p'_B] \approx [0.837, 0.857]$ assuming $q = 0.9$ (or, equivalently, 0.1), as shown in Figs. 5(b) and 5(c). We have experimentally generated the GWSs for $p = 0.8$ and 0.9 , but unfortunately they are outside the desired range $[p'_{S_2}, p'_B]$.

To solve this problem, we recall that mixtures of any two GWSs, say, $\rho_{\text{GW}}(p_1, q)$ and $\rho_{\text{GW}}(p_2, q)$ for a fixed value of q , are also GWSs. Specifically,

$$\rho_{\text{GW}}^E(p, q) = \frac{p_2 - p}{p_2 - p_1} \rho_{\text{GW}}(p_1, q) + \frac{p - p_1}{p_2 - p_1} \rho_{\text{GW}}(p_2, q). \quad (22)$$

Thus, we can use this property to produce (or simulate) a GWS, which was not measured directly in our experiment, e.g.,

$$\rho_{\text{GW}}(0.85, q) = \frac{1}{2} [\rho_{\text{GW}}^E(0.8, q) + \rho_{\text{GW}}^E(0.9, q)], \quad (23)$$

simply by balanced postmeasurement numerical mixing of the two experimental GWSs $\rho_{\text{GW}}^E(p, q)$ for $p = 0.8$ and 0.9 assuming $q = 0.9$. We refer to this method as a hybrid experimental generation, as written in Table II for regime 4. By contrast to this regime, we have *directly* generated experimental states in all other regimes listed in Tables I and II. Moreover, all the states plotted in our figures correspond to those directly generated experimentally without using any postmeasurement numerical mixing.

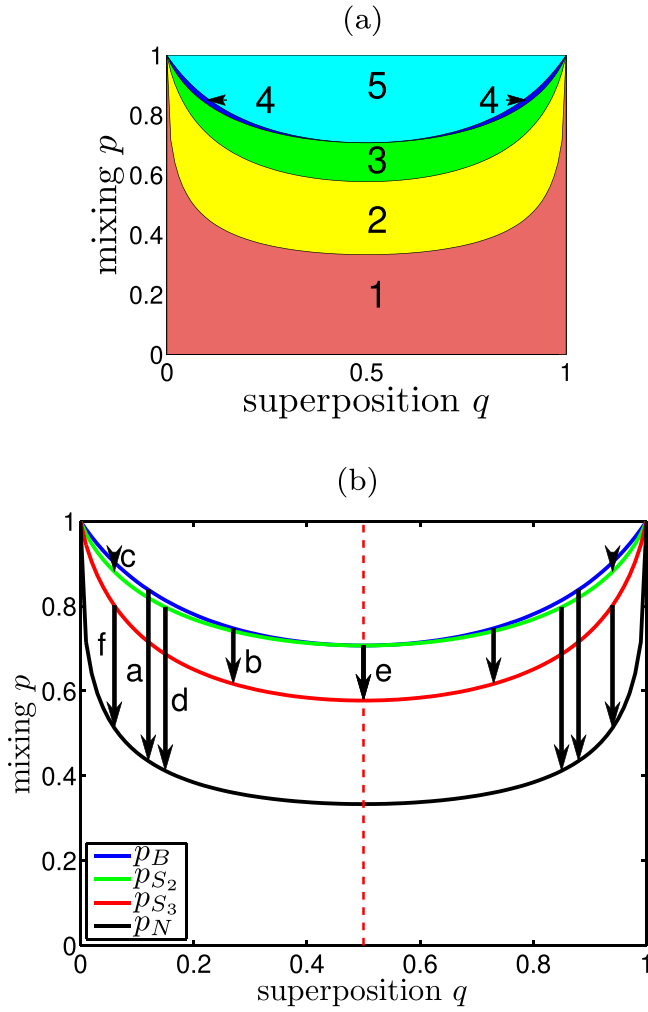


FIG. 6. Threshold mixing parameters $p_i(q)$ versus the superposition parameter q for the GWSs. (a) The threshold curves separate the five regimes in the hierarchy of the classes of quantum correlations, which are listed in Table II. (b) Transitions between various curves, requiring the largest amount of white noise, are indicated by arrows. It can be seen that the only arrow e for the Werner states (i.e., the GWSs at $q = \frac{1}{2}$) is marked for the transition between the curves $p_{S_2}(q)$ and $p_{S_3}(q)$. All the other arrows are plotted at $q \neq \frac{1}{2}$. This explains the meaning of enhanced robustness of the Bell-nondiagonal GWSs against the white noise compared to that of the Werner states. The locations at q_{opt} and the lengths of the labeled arrows are listed in Table III. The unlabeled arrows are located at $q'_{\text{opt}} = 1 - q_{\text{opt}}$.

Our prediction of the existence of states in regime 4 is a surprising result and our experiment just confirms it. This prediction seems to be especially counterintuitive in the context of the Girdhar-Cavalcanti article in [89] (see also Refs. [90,91]), which seemingly implies the impossibility of generating states in this regime. However, the Girdhar-Cavalcanti theorem is valid in a 2-2 measurement scenario only, i.e., for “a scenario employing only correlations between two arbitrary dichotomic measurements on each party” [89]. Our steering measures S_2 and S_3 refer to 2-3 and 3-3 measurement scenarios, respectively. Indeed, we always assume a full tomography on Bob’s side corresponding to the measurement of the three Stokes parameters $\langle \sigma_x \rangle$, $\langle \sigma_y \rangle$, and

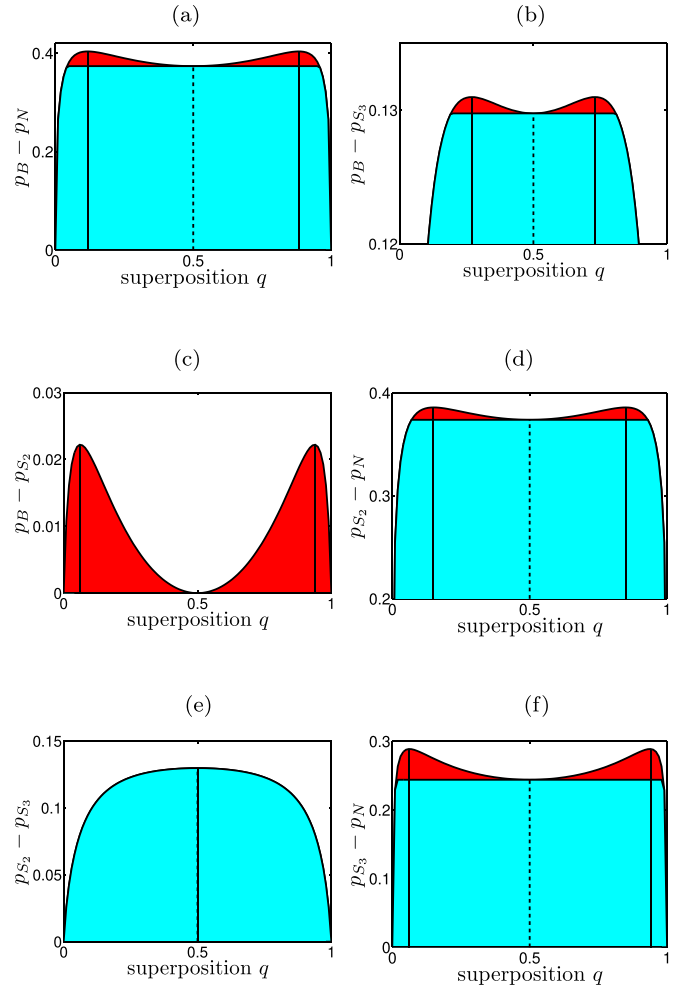


FIG. 7. Differences $\Delta_{ij}(q) = p_i(q) - p_j(q)$ of the threshold mixing parameters versus the superposition parameter q for the GWSs corresponding to the transitions shown by the arrows in Fig. 6. The red-colored regions show explicitly the improved robustness against the white noise of the Bell-nondiagonal GWSs compared to the diagonal ones in the Bell basis (i.e., the standard Werner states), except the case shown in (e). Combined red and cyan regions correspond to the regimes listed in Table II. Panels show: (a) entangled states without nonlocality, corresponding to regimes 2–4; (b) 3MS-steerable states without nonlocality, regimes 3 and 4; (c) 2MS-steerable states without nonlocality, regime 4; (d) 2MS-unsteerable entangled states, regimes 2 and 3; (e) steerable states in 3MS but not in 2MS, regime 3; and (f) 3MS-unsteerable entangled states, regime 2.

$\langle \sigma_z \rangle$, while the projective measurements on Alice’s side can be limited to 2MS or 3MS. It is seen that our and Girdhar and Cavalcanti’s steering results refer to different measurement scenarios. Thus, the observation of regime 4 in our steering scenarios does not imply the violation of the Girdhar-Cavalcanti theorem.

B. Increased robustness against white noise of Bell-nondiagonal generalized Werner states

Even a quick analysis of Figs. 6(b) and 7 and Table III shows one of the main theoretical results of this paper,

TABLE III. Transitions between the threshold values of different correlations of the GWSs for the optimal superposition parameter q_{opt} , which maximizes the white-noise robustness $\Delta_{if}(q_{\text{opt}}) = p_i(q_{\text{opt}}) - p_f(q_{\text{opt}})$ for $i \neq f \in \{N, S_2, S_3, N\}$. These transitions correspond to the arrows shown in Fig. 6(b), and the length of a given arrow is given by $\Delta_{if}(q_{\text{opt}})$. The parameter p_i (p_f) is the threshold value of the mixing parameter p for the initial (final) class of correlations or, equivalently, the position of the beginning (end) of the corresponding arrow. The last column shows the relative robustness with respect to the standard Werner states (i.e., the GWS for $q = \frac{1}{2}$). Note that, for every q_{opt} , there is a second optimal value of the superposition parameter, $q'_{\text{opt}} = 1 - q_{\text{opt}}$, exhibiting the same quantum correlation properties.

Transition	q_{opt}	$p_i(q_{\text{opt}})$	$p_f(q_{\text{opt}})$	$\Delta_{if}(q_{\text{opt}})$	$\Delta_{if}(\frac{1}{2})$	$\Delta_{if}(q_{\text{opt}}) - \Delta_{if}(\frac{1}{2})$
(a) $p_B \rightarrow p_N$	0.1170	$p_B = 0.8412$	$p_N = 0.4375$	0.4037	0.3738	0.0299
(b) $p_B \rightarrow p_{S_3}$	0.2692	$p_B = 0.7481$	$p_{S_3} = 0.6171$	0.1310	0.1298	0.0012
(c) $p_B \rightarrow p_{S_2}$	0.0625	$p_B = 0.9001$	$p_{S_2} = 0.8779$	0.0222	0	0.0222
(d) $p_{S_2} \rightarrow p_N$	0.1508	$p_{S_2} = 0.7971$	$p_N = 0.4113$	0.3858	0.3738	0.0120
(e) $p_{S_2} \rightarrow p_{S_3}$	0.5000	$p_{S_2} = 0.7071$	$p_{S_3} = 0.5774$	0.1298	0.1298	0
(f) $p_{S_3} \rightarrow p_N$	0.0630	$p_{S_3} = 0.7959$	$p_N = 0.5071$	0.2888	0.2440	0.0448

i.e., increased robustness against the white noise of Bell-nondiagonal GWSs compared to the standard (Bell-diagonal) Werner states. Below we give a more intuitive and detailed explanation of this result.

We recall that Bell diagonal (nondiagonal) GWSs are the maximally (partially) entangled states affected by white noise. Let us analyze the amount of white noise (i.e., $1 - p$) which is necessary to make the transition of a GWS from one threshold value, say, $p_i(q)$, to another (final) value, $p_f(q)$, for a given value of the superposition parameter q . Thus, the required white noise can be quantified by

$$\Delta_{if}(q) \equiv p_i(q) - p_f(q) \quad (24)$$

for $i \neq f \in \{N, S_3, S_2, B\}$, which is plotted in Fig. 7 and numerically given in Table III.

For example, let us consider the maximally entangled Werner state admitting an LHV model, i.e., $\rho_W(p_B)$. Our question is about the minimum amount of white noise which should be added to this state to make it separable, i.e., $\rho_W(p_N)$. The answer is $\Delta_{BN}(q = \frac{1}{2}) = 1/\sqrt{2} - \frac{1}{3} \approx 0.3738$. We find that, in the case of the GWSs, the minimum amount of white noise needed to convert the maximally entangled GWS $\rho_{\text{GW}}[p_B(q), q]$, admitting an LHV model, to the closest separable state $\rho_{\text{GW}}[p_N(q), q]$ can be larger than that for the Werner states, $\Delta_{BN}(q) > \Delta_{BN}(\frac{1}{2})$, for some values of the superposition parameter q corresponding to the red regions in Fig. 7(a). Assuming that $q = 0.9$ (as set in our experiments), we obtain $\Delta_{BN}(0.9) = 0.4029 > 0.3738$. Actually, the largest value $\max_q \Delta_{BN}(q) = \Delta_{BN}(q') = 0.4037$ can be achieved for $q' = 0.8829$ and $1 - q'$, which can be calculated by solving the sixth-order equation $(1 + 4x^2)^3 = x^2(1 + 4x)^4$ with $x = \sqrt{q'(1 - q')}$.

The same conclusion about higher robustness of the Bell-nondiagonal GWSs against white noise compared to that of the Werner states can also be drawn for other transitions, indicated by the arrows in Figs. 6(b) and 7 and also listed in Table III. The only exception is observed for the transition corresponding to $\Delta_{S_2, S_3}(q)$, which reaches the largest value for the Werner states, as shown in Fig. 7(e).

More white noise should be added to a Bell state to reach any threshold value p_j compared to that for any partially entangled state, because $1 - p_j(\frac{1}{2}) > 1 - p_j(q)$ for $q \neq \frac{1}{2}$ and $j \in \{N, S_3, S_2, B\}$, i.e., the amount of white noise destroying

completely any quantum properties of the states, including entanglement, steering, and nonlocality. So, in that sense, the Werner states are more robust against white noise than the nondiagonal GWSs. However, by choosing proper reference states or proper transitions, one can draw the opposite conclusion, as we have demonstrated in this section and clearly visualized in Figs. 6(b) and 7.

C. Increased robustness of steering for a larger number of measurements

Our paper is focused on analyzing steering in only the two- and three-measurement scenarios. Nevertheless, in Appendix D we also discuss steering in multimeasurement scenarios including the case of steering in the limit of an infinite number of types of available measurements.

Specifically, we analyze lower and upper bounds on steering for a much larger number n of measurements (even $n = 136$). We demonstrate that entangled GWSs, which are unsteerable for a very large (or in principle infinite) number of measurements, can be more robust against white noise if they are nondiagonal in the Bell-state basis compared to the diagonal ones (i.e., the Werner states).

First, we recall that, while the analyzed entanglement measures reveal the property of a given state independent of its measurements, the measures for steerability and Bell nonlocality additionally depend on the available measurements. Thus, one can raise the following questions. (i) Is a larger spread (corresponding to higher robustness) between different classes of correlations in the GWSs an artifact stemming from the fact that the considered steering and Bell-nonlocality measures perform better on less entangled states? This question can also be rephrased: (ii) Can one expect to find the same robustness behavior for some tight bounds for Bell nonlocal states and steerable states (taking into account any measurement scenario)?

We answer these questions by calculating tight upper (p_S^{up}) and lower (p_S^{low}) bounds on steering for the GWSs for a large number of measurements. These numerical bounds strongly suggest that the hierarchy also holds for an arbitrary number of measurements. Indeed, similar analysis can be performed for Bell nonlocality of the GWSs, as discussed in [68], to show that the Horodecki measure fully describes the nonlocality in

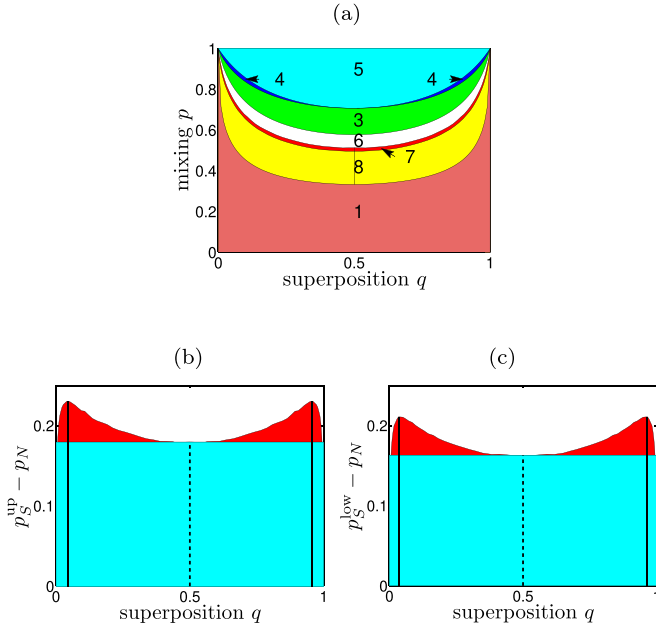


FIG. 8. (a) Same as in Fig. 6(a) but with additional regions (regimes) 6–8 of steerability in the limit of a large number of measurements. Also shown are the differences (b) $p_S^{\text{up}} - p_N$ and (c) $p_S^{\text{low}} - p_N$, where p_N is given by Eq. (16): (b) supremum of unsteerable entangled states, regimes 7 and 8, and (c) unsteerable entangled states, regime 8. The curve p_S^{up} is the border between regimes 6 and 7, which corresponds to a sufficient condition for steerability of Ref. [7], while the curve p_S^{low} is the border between regimes 7 and 8, which corresponds to a sufficient condition of unsteerability based on the algorithm and numerical data of Refs. [68,69] assuming 136 projective measurements. Panels (b) and (c) show, analogously to those in Fig. 7, that the optimal robustness of steering assuming a large number of measurements compared to the entanglement of the GWSs is observed for the Bell-nondiagonal GWSs with the superposition parameter $q \neq \frac{1}{2}$ (as denoted by solid blue lines).

two-qubit states with no restriction on the number of measurements.

Two bounds on multimeasurement steering are shown in Fig. 8. Specifically, the upper bound p_S^{up} , which corresponds to the border curve between regimes 6 and 7 in Fig. 8(a), is a sufficient condition for the steerability of the GWSs. This bound was obtained numerically in Refs. [68,69] from a criterion of Ref. [7] using an SDP technique for 13 measurements on the Bloch sphere. Moreover, the lower bound p_S^{low} , which is shown by the curve between regimes 7 and 8, corresponds to a sufficient condition of the unsteerability of the GWSs based on the algorithm of Refs. [68,69] for constructing LHS models assuming 136 projective optimal (or almost optimal) measurements corresponding to the fourth level of their algorithm. The curves for both p_S^{low} and p_S^{up} are plotted using the numerical data of Ref. [69]. Thus, any GWS above the p_S^{up} curve in Fig. 8(a) is steerable, while any state below the p_S^{low} curve is unsteerable. The unsteerability of some of the states in regime 7 (lying close to the border curve p_S^{low}) can be tested by applying the algorithm of Refs. [68,69] for higher levels, which corresponds to analyzing a larger number of measurements ($n \gg 136$). However, it is unclear whether any

GWSs lying inside regime 7 can be steerable in the limit of $n \rightarrow \infty$.

Figure 8(a) shows that by including the criteria for steering in multimeasurement scenarios, in addition to S_2 and S_3 , one can study a CC hierarchy which is more refined than that in Fig. 6(a). Note that regime 2 in Fig. 6(a) corresponds to the sum of regimes 6–8 shown in Fig. 8(a).

To answer the questions raised above, we plot the differences $p_S^{\text{up}} - p_N$ and $p_S^{\text{low}} - p_N$ in Figs. 8(b) and 8(c), respectively. Both figures are quite similar and show that the optimal robustness against noise is observed for the Bell nondiagonal GWSs with the superposition parameter $q \neq \frac{1}{2}$ (denoted by black solid lines). Thus, even without knowing the exact threshold values between the steerability and unsteerability of the GWSs in the limit of an infinite number of measurements, one can conclude that the predicted optimal robustness is *not* an artifact, at least for the cases shown in Figs. 8(b) and 8(c). This is the answer to question (i). Concerning question (ii), the robustness behavior is different for different $p_i = p_S^{\text{up}}, p_S^{\text{low}}, p_{S_2}, p_{S_3}$. Indeed, the optimal values of the superposition parameter q maximizing $p_i - p_N$ depend on i . However, this property does not weaken our conclusion about higher robustness against the white noise of some Bell nondiagonal GWSs compared to that of the Werner states.

VII. CONCLUSION

The main purpose of this work was to analyze a CC hierarchy of theoretical and experimental Werner states and their generalization, i.e., the Bell-nondiagonal GWSs. We recall that the considered GWSs are the mixtures of partially entangled two-qubit pure states (not only of a Bell state) and the maximally mixed state (white noise). We have shown that the Bell-nondiagonal GWSs exhibit a more refined CC hierarchy compared to that of the Bell-diagonal GWSs, i.e., the Werner states.

By tuning the mixing and superposition parameters of the GWSs, we have experimentally generated and tomographically reconstructed such GWSs, which reveal the hierarchy of the following classes of correlations: 1, separability; 2, entanglement without steerability in the 3MS; 3, steerability in the 3MS but not steerable in the 2MS; 4, steerability in the 2MS without violating the Bell-CHSH inequality (so admitting LHV models); and 5, Bell nonlocality, which cannot be explained within LHV models. Note that the case of steering is a little more subtle since the measures assume specific measurements. Thus, we have also analyzed a sufficient condition for unsteerability assuming a very large number (i.e., 136) of measurements.

In particular, we found five different parameter regimes of the GWSs, including the states which are steerable in a 2MS without violating Bell inequalities and thus corresponding to regime 4. This is a counterintuitive result, especially when compared with the Girdhar-Cavalcanti theorem [89], which states that “[all] two-qubit states that are steerable via CHSH-type correlations are Bell nonlocal” [89]. In Sec. VIA we explained why the observation of regime 4 in our steering scenarios does not imply the violation of the Girdhar-Cavalcanti theorem. We also demonstrated that regime 4 cannot be observed for the usual Werner states.

Moreover, we have shown that the robustness against the white noise for, e.g., steerable states admitting LHV models can be stronger for some Bell-nondiagonal GWSs than that for the diagonal GWSs (i.e., the Werner states). This can be achieved by properly choosing the value of the superposition coefficient q , as shown in Figs. 6(b) and 7. Thus, we addressed the problem of optimal robustness of states against white noise. Specifically, we analyzed threshold values (curves) separating the five regimes of quantum correlations. Then we could find optimal transitions between various curves corresponding to the largest amount of white noise or, in other words, to the largest spread in the hierarchy. Thus, we discovered the optimal Bell-nondiagonal GWSs which are more robust against white noise than the Werner states.

Furthermore, we considered lower and upper bounds on steering in multimeasurement scenarios. Again we demonstrated better robustness against the white noise of some unsteerable entangled Bell-nondiagonal GWSs compared to the diagonal ones. Thus, such enhanced robustness is not limited to only the two- and three-measurement steering scenarios; it can also be observed for steering in the limit of a large number of measurements.

Possible applications of the discovered optimal robustness against white noise can be found for quantum cryptography. For instance, imagine that legitimate users of some secure quantum communications system want to use steering (or entanglement) such that it should not be detected by the violations of Bell inequalities by others. Thus, assuming that the communication is via a depolarizing channel, it is convenient to use partially steerable (or partially entangled) states which are Bell local and are the most robust against white noise. Such optimal states are indicated by arrows in Fig. 6(b).

Our study of the hierarchy of the classes of spatial quantum correlations can be generalized to analyze a hierarchy of their temporal or spatiotemporal analogs. Indeed, the concepts of spatial and temporal quantum correlations are closely related. Formally, it is enough to replace two-qubit measurements for testing spatial correlations by measurements on a single qubit, followed by transmission through a channel, to reveal temporal correlations, as explained in the example of spatial and temporal steering in Ref. [65]. Thus, many of the results discussed here for spatial correlations can also be generalized to temporal correlations. We explicitly indicated such relations in various sections of this paper. Analyses of CC hierarchies of temporal correlations can lead to a deeper understanding of, e.g., quantum causality [92] or enable designing new types of quantum cryptosystems and finding new methods of breaking the standard ones.

We believe that analyzing such CC hierarchies is interesting concerning both fundamental aspects of quantum mechanics and possible cryptographic applications for, e.g., secure communication, secure information retrieval, and zero-knowledge proofs of (quantum) identity.

ACKNOWLEDGMENTS

We acknowledge helpful discussions with Huan-Yu Ku, K.J., K.B., and K.L. acknowledge financial support from the Czech Science Foundation through Project No. 20-17765S. The authors also acknowledge Project No.

CZ.02.1.01/0.0/0.0/16_019/0000754 of the Ministry of Education, Youth, and Sports of the Czech Republic. K.J. also acknowledges the Palacký University internal Grant No. IGA-PrF-2021-004. A.M. was supported by the Polish National Science Centre under the Maestro Grant No. DEC-2019/34/A/ST2/00081.

APPENDIX A: UNIVERSAL DETECTION OF QUANTUM CORRELATIONS WITHOUT FULL QUANTUM STATE TOMOGRAPHY

In this work we determined quantum correlations from experimentally generated and reconstructed states using a full QST. Here we address the question of universal detection of quantum correlations without full QST.

Universal detection of an entanglement measure without QST. The first experimental universal detection of standard two-qubit entanglement without full QST was proposed in Ref. [60] (see also [93]) based on the universal witness of Ref. [61]. This method was later improved in Ref. [94] to show theoretically a direct experimental method for determining the negativity of a general two-qubit state based on 11 measurements performed on multiple copies of the state using Hong-Ou-Mandel interference. None of these methods of universal entanglement detection without a full state tomography has been demonstrated experimentally yet because of the complexity of such setups and low probability of required multiple coincidences. Note that experimental detection, without a complete tomography of the fully entangled fraction of Bennett *et al.* [95], was demonstrated by us in Ref. [75]. Unfortunately, the fully entangled fraction is not a universal entanglement witness in general, so it usually only gives a sufficient (but not necessary) condition of entanglement.

Universal detection of a steering measure without QST. Such methods have not been implemented or even proposed for the steering robustness or the steerable weight. The calculations of these popular steering measures for general states are based on numerical optimization (using semidefinite programs). Thus, in general, these measures could only be determined experimentally for tomographically reconstructed states or processes, as it has been done in dozens of experimental works (see reviews [7,8] and references therein). Of course, there are many experiments demonstrating quantum steering via nonuniversal witnesses (to reveal a hierarchy of criteria), i.e., by observing the violations of steering inequalities [7,8]. We note that measures of steering (e.g., that proposed for a 2MS and a 3MS in Ref. [91]) which are based on the maximal violation of well-established steering inequalities can be measured without a complete QST. For example, the optimal violation of the Cavalcanti-Jones-Wiseman-Reid inequality [96] can in principle be experimentally demonstrated with polarized photons without scanning all the angles of polarizers. This can be done, as we anticipate, in systems similar to those demonstrating the Horodecki measure of Bell nonlocality [75].

Universal detection of a nonlocality measure without QST. The Horodecki measure [70,71]) of Bell-CHSH nonlocality of two-qubit states can indeed be measured without a full QST, but it was first determined experimentally only recently in our experiment [75] without scanning the angles of the

polarizers to obtain an optimal value of the angles maximizing the violation of the Bell-CHSH inequality for an unknown two-qubit state. To demonstrate the power of this method, we have implemented an entanglement-swapping device with which we universally detected experimentally a nonlocality measure (without scanning the polarization angles or without *a priori* information about a given generated state).

APPENDIX B: STEERABLE WEIGHT IN A THREE-MEASUREMENT SCENARIO

Here we consider two-qubit EPR steering in a 3MS, when Alice performs the measurements of the three Pauli operators $X = |+\rangle\langle+| - |-\rangle\langle-|$, $Y = |R\rangle\langle R| - |L\rangle\langle L|$, $Z = |0\rangle\langle 0| - |1\rangle\langle 1|$, of qubits encoded in the polarization states of photons, as in our experiment. Thus, these measurements are just the projections onto the Pauli-operator eigenstates $|\pm\rangle = (|0\rangle \pm |1\rangle)/\sqrt{2}$, $|R\rangle = (|0\rangle + i|1\rangle)/\sqrt{2}$, $|L\rangle = (|0\rangle - i|1\rangle)/\sqrt{2}$, $|0\rangle$, and $|1\rangle$, which correspond to the diagonal, anti-diagonal, right-circular, left-circular, horizontal, and vertical polarization states, respectively. These measurements of Alice generate unnormalized states $\sigma_{a|x}$ of Bob for $x = X, Y, Z$ assuming measured eigenvalues $a = \pm 1$. By defining $f(|m\rangle) = \text{Tr}_A[(|m\rangle\langle m| \otimes I)\rho]$, the six possible unnormalized Bob states $\sigma_{a|x}$ read

$$\begin{aligned} \sigma_{+1|X} &= f(|+\rangle), & \sigma_{-1|X} &= f(|-\rangle), \\ \sigma_{+1|Y} &= f(|R\rangle), & \sigma_{-1|Y} &= f(|L\rangle), \\ \sigma_{+1|Z} &= f(|0\rangle), & \sigma_{-1|Z} &= f(|1\rangle). \end{aligned} \quad (\text{B1})$$

Alice, after performing her measurements, holds a classical random variable $\lambda \equiv [x, y, z] = [\langle x|X|x\rangle, \langle y|Y|y\rangle, \langle z|Z|z\rangle]$, with hereafter $x, y, z = \pm 1$. Thus, the variable λ can take the values $\lambda_1 = [-1, -1, -1]$, $\lambda_2 = [-1, -1, 1]$, \dots , $\lambda_8 = [1, 1, 1]$. The unsteerable assemblage $\sigma_{a|x}^{\text{us}}$, can now be expressed as $\sigma_{\pm 1|X}^{\text{us}} = \sum_{y,z} \sigma_{\pm 1,y,z}$, $\sigma_{\pm 1|Y}^{\text{us}} = \sum_{x,z} \sigma_{x,\pm 1,z}$, and $\sigma_{\pm 1|Z}^{\text{us}} = \sum_{x,y} \sigma_{x,y,\pm 1}$, where $\sigma_\lambda \equiv \sigma_{xyz}$ are the states held by Bob. The steerable weight S_3 in our 3MS can be given by the solution of the SDP

$$S_3 = 1 - \max \text{Tr} \sum_{x,y} \sigma_{xyz} \quad (\text{B2})$$

such that $\sigma_{xyz} \geq 0$ and

$$\begin{aligned} \sigma_{\pm 1|X} - \sum_{y,z} \sigma_{\pm 1,y,z} &\geq 0, \\ \sigma_{\pm 1|Y} - \sum_{x,z} \sigma_{x,\pm 1,z} &\geq 0, \\ \sigma_{\pm 1|Z} - \sum_{x,y} \sigma_{x,y,\pm 1} &\geq 0. \end{aligned} \quad (\text{B3})$$

APPENDIX C: STEERABLE WEIGHT IN TWO-MEASUREMENT SCENARIOS

The above approach can be simplified when analyzing EPR steering in 2MSs, i.e., when Alice is performing the measurements of only two Pauli operators (XY , XZ , and YZ). Thus, one can consider the following three measures.

(i) For the steerable weight S_2^{XY} for the measurements of X and Y , the corresponding unsteerable assemblage $\sigma_{a|x}^{\text{us}}$ can be expressed as $\sigma_{\pm 1|X}^{\text{us}} = \sum_y \sigma_{\pm 1,y}$ and $\sigma_{\pm 1|Y}^{\text{us}} = \sum_x \sigma_{x,\pm 1}$, where $\sigma_\lambda \equiv \sigma_{xy}$ are the states held by Bob. Then the corresponding steerable weight S_2^{XY} can be calculated as the solution of the SDP

$$S_2^{XY} = 1 - \max \text{Tr} \sum_{x,y} \sigma_{xy}, \quad (\text{C1})$$

under the constraints $\sigma_{xy} \geq 0$ and

$$\sigma_{\pm 1|X} - \sum_y \sigma_{\pm 1,y} \geq 0, \quad \sigma_{\pm 1|Y} - \sum_x \sigma_{x,\pm 1} \geq 0. \quad (\text{C2})$$

(ii) The steerable weight S_2^{XZ} , based on Alice's measurements of the Pauli operators X and Z , is given by

$$S_2^{XZ} = 1 - \max \text{Tr} \sum_{x,z} \sigma_{xz} \quad (\text{C3})$$

such that $\sigma_{xz} \geq 0$ and

$$\sigma_{\pm 1|X} - \sum_z \sigma_{\pm 1,z} \geq 0, \quad \sigma_{\pm 1|Z} - \sum_x \sigma_{x,\pm 1} \geq 0. \quad (\text{C4})$$

(iii) The steerable weight S_2^{YZ} corresponding to measuring the Pauli operators Y and Z can be calculated as

$$S_2^{YZ} = 1 - \max \text{Tr} \sum_{y,z} \sigma_{y,z}, \quad (\text{C5})$$

under the conditions $\sigma_{yz} \geq 0$ and

$$\sigma_{\pm 1|Y} - \sum_z \sigma_{\pm 1,z} \geq 0, \quad \sigma_{\pm 1|Z} - \sum_y \sigma_{y,\pm 1} \geq 0. \quad (\text{C6})$$

The optimized 2MS steerable weight (S_2) can be given as the maximum value of the steerable weights for specific measurement choices, i.e.,

$$S_2 = \max (S_2^{XY}, S_2^{XZ}, S_2^{YZ}). \quad (\text{C7})$$

This definition of S_2 can directly be applied to symmetric states, including the Werner states and GWSs. However, for nonsymmetric states (including some of our experimental density matrices), the optimal projectors can be found numerically by maximizing the steerable weight over unitary transformations for any two Pauli operators. In our experiments and theoretical analysis, we apply only single Pauli operators (rather than their linear combinations) and then optimize them over their unitary transformations. Thus, we obtain the steerable weights, which are optimized over von Neumann's projection-valued measures, instead of the most general case of POVMs. Note that the required optimization over POVMs is more demanding both experimentally and theoretically and it is not applied in this work. We find that, on the scale of Figs. 4(c) and 5(c), no differences can be seen for S_2 if it is calculated by the optimized projectors and by applying directly Eq. (C7) for any of the measured states.

Note that, in this approach to determine S_2 , we are limiting the number of types of measurements on Alice's side, but a full QST is always assumed on Bob's side corresponding to measuring all the Pauli operators. Thus, the steerable weight S_3 corresponds to a 3-3 measurement scenario, i.e., three types of measurements on Alice's and Bob sides (assuming that the

efficiency of detectors is known), while the steerable weight S_2^{ij} (for the specific choice of two Pauli operators) corresponds to a 2-3 scenario, i.e., based on two types of measurements on Alice's side and three on Bob's side.

All these steerable weights in the two- and three-measurement scenarios can be efficiently calculated numerically as solutions of the described semidefinite programs using standard numerical packages for convex optimization. Our numerical programs are based on the software for disciplined convex programming of Ref. [97]. The steerable weights in our work were calculated using experimental density matrices, which were reconstructed using a full quantum tomography.

APPENDIX D: STEERABILITY IN MULTIMEASUREMENT SCENARIOS

A related question arises about the steerability using a larger number n of types of measurements on Alice's side, especially in the limit of an infinite number of measurements. The algorithms of Refs. [68,69,98] for constructing LHS models can be applied to arbitrary entangled states and thus can be used for finding numerically a sufficient condition of unsteerability (i.e., a lower bound on steerability) based on a given number of projective measurements. Note that for the GWSs, such a lower bound on steerability was determined up to $n = 136$ measurements in Ref. [69]. For convenience, we consider here a steering lower bound $p_S^{\text{low}}(n)$, which can be numerically determined by the protocols of Refs. [68,69] for a given number n of measurements. We also consider a steering upper bound $p_S^{\text{up}}(n)$, being a sufficient condition for steerability, based on an SDP technique of Ref. [7] (see also [69]) assuming specifically 13 measurements on the Bloch sphere.

The algorithm of Refs. [68,69] has already been applied to the steerability of the Bell-diagonal states (including the Werner states) and GWSs (there referred to as partially entangled states with white noise). Sufficient conditions of unsteerability, corresponding to $n = 6, 16, 46$, and 136 types of measurements, were found for four levels of the algorithm [69]. These results can enable calculating $p_S^{\text{low}}(n)$. Note that each type of measurement is characterized by a Bloch vector and all such vectors form a polyhedron on the Bloch sphere.

It is quite challenging to numerically calculate the lower bound $p_S^{\text{low}}(n)$ of steerability in multimeasurement scenarios, even for the next layer of the protocol of Fillettaz *et al.* [69] (corresponding to the number of measurements greater than 136) because of the problem which is closely related to the ‘‘curse of dimensionality.’’ Indeed, the number of deterministic strategies to be checked numerically grows exponentially with the number of measurements. The results should also be optimized for the orientation of the polyhedra; otherwise the results differ significantly, as explicitly shown in Ref. [68].

The ranges of the allowed values of the mixing (p) and superposition (q) parameters in $\rho_{\text{GW}}(p, q)$, for which the GWSs are steerable, increase with the number of measurements n . Thus, finding numerically a solution to these steering problems could in principle enable us to analyze a more refined hierarchy of the classes of steerability as a function of the number of measurements such that a given state is steerable

using a given number of measurements, but unsteerable using a smaller number of measurements. However, an experimental demonstration of such a refined hierarchy is quite challenging, as explained below.

Clearly, a direct experimental demonstration that a given state is indeed unsteerable based on 136 types of measurements is extremely demanding using linear optics. However, even theoretical demonstration of such a refined hierarchy of the classes of multimeasurement steerability for tomographically reconstructed experimental states is quite challenging. These problems include the following.

First problem. We recall that our experimental GWSs $\rho_{\text{GW}}^E(p, q)$ have a high Bures fidelity F compared to the theoretical optimal GWSs $\rho_{\text{GW}}(p_{\text{opt}}, q_{\text{opt}})$ which on average are equal to 0.97. Nevertheless, $\rho_{\text{GW}}^E(p, q)$ and $\rho_{\text{GW}}(p_{\text{opt}}, q_{\text{opt}})$ can still have very different steering properties such that one of the states is steerable and the other is unsteerable in the same n -measurement scenario, especially for $n > 3$.

Note that all the examples of multimeasurement steerability, based on the protocols of Refs. [68,69,98], were numerically tested only for highly symmetric states (including the Werner states and GWSs). Unfortunately, our experimental states ρ_{GW}^E have usually a broken symmetry compared to that of the theoretical GWSs ρ_{GW} . So the calculation of the steerability of ρ_{GW}^E in the 2MS and 3MS is sometimes much more time consuming and less precise. This is even the case for calculating the steerable weight and steering robustness using standard packages in the 2MS. For example, the calculations of these two steering measures for ρ_{GW} take at most a few seconds on a standard PC, while those for the generated ρ_{GW}^E require sometimes dozens of minutes, assuming the same precision in both cases. These numerical problems grow very fast with the increasing number n of measurements.

Second problem. Our experimental tuning of the parameters p and q for the GWSs is not fine enough, as explained in greater detail in Sec. IV. Note that the ranges of parameters p and q of the GWSs are very small such that a given GWS is steerable with $n + 1$ measurements and unsteerable with n measurements for $n > 3$. Our experimental tuning of p and q was good enough to directly generate states in regime 3 corresponding to $S_3 > 0$ and $S_2 = 0$. However, we were not able to directly generate experimentally GWSs belonging to different regimes of steerability for a larger number n . Note that even our experimental GWS in regime 4, corresponding to $S_2 > 0$ and $B = 0$, was not generated directly. Indeed, we obtained it in a hybrid way, i.e., by numerically mixing experimental states belonging to other regimes, as explained in Sec. VI.

Third problem. It is numerically very challenging to check whether a given ρ_{GW}^E is n -measurement steerable and $(n - 1)$ -measurement unsteerable, which is crucial in experimentally demonstrating such a refined hierarchy of the steerability classes for multimeasurement scenarios. Specifically, if we numerically obtain $S_n(\rho_{\text{GW}}^E) \sim 10^{-12}$, which is the precision of our numerical calculation of the steering measures, it is quite biased to decide whether this state ρ_{GW}^E is indeed steerable or not. With the increasing number n of measurements, the numerically estimated $S_n(\rho_{\text{GW}}^E)$ become less and less precise. So the question arises how to correctly classify the steerability of a given experimental state in the hierarchy of classes of steerability in various multimeasurement scenarios.

Fourth problem. The border between the steerable and unsteerable theoretical GWSs is not precisely determined in the limit of an infinite number n of measurements on Alice's side. Indeed, the border corresponds to region 7 in Fig. 8(a) spanned by the curves p_S^{low} and p_S^{up} . Estimating p_S^{low} for our experimental imperfect GWSs ρ_{GW}^E is even more demanding because ρ_{GW}^E usually exhibits a broken symmetry compared to that of the ideal GWSs ρ_{GW} .

Thus, for these numerical and experimental reasons, we have decided to analyze in detail the steerability of our experimental states for the two simplest types of measurement scenarios only. We believe that this is good enough to show the hierarchy of some classes of correlations (including steerability in 2MS and 3MS) for experimental states.

APPENDIX E: HIERARCHY OF ENTANGLEMENT CRITERIA

1. Hierarchy of the Shchukin-Vogel entanglement criteria

Here we briefly recall the Shchukin-Vogel entanglement criteria for the universal detection of distillable entanglement via the matrices of moments of the annihilation and creation operators [43]. This approach, in principle, does not require a full QST, so it is an alternative to the approach applied in our experiment using QST. We indicate some advantages and drawbacks of this approach for detecting two-qubit entanglement.

The Shchukin-Vogel criteria are based on the Hermitian matrices of moments for a given two-mode state ρ , which are defined as

$$\mathcal{M}_N^{\text{org}} = \begin{bmatrix} M_{11} & M_{12} & \cdots & M_{1N} \\ M_{21} & M_{22} & \cdots & M_{2N} \\ \cdots & \cdots & \cdots & \cdots \\ M_{N1} & M_{N2} & \cdots & M_{NN} \end{bmatrix}, \quad (\text{E1})$$

where $M_{ij} = \langle (a^{\dagger i_2} a^{i_1} b^{\dagger i_4} b^{j_3}) (a^{\dagger j_1} a^{j_2} b^{\dagger j_3} b^{j_4}) \rangle$ are the moments of the annihilation (a and b) and creation (a^\dagger and b^\dagger) operators of two modes of arbitrary dimension. Here i and j label multi-indices, e.g., (i_1, i_2, i_3, i_4) . These moments can be detected experimentally (at least for not too high powers) using, e.g., the setup based on homodyne detection as described by Shchukin and Vogel [99]. A partially transposed matrix of moments can be obtained from $\mathcal{M}_N^{\text{org}}$ as

$$\begin{aligned} M_{ij}^\Gamma &= \langle (a^{\dagger i_2} a^{i_1} a^{\dagger j_1} a^{j_2}) (b^{\dagger i_4} b^{j_3} b^{\dagger j_3} b^{j_4}) \rangle^\Gamma \\ &= \langle (a^{\dagger i_2} a^{i_1} a^{\dagger j_1} a^{j_2}) (b^{\dagger i_4} b^{j_3} b^{\dagger j_3} b^{j_4}) \rangle^\dagger \\ &= \langle (a^{\dagger i_2} a^{i_1} a^{\dagger j_1} a^{j_2}) (b^{\dagger j_4} b^{j_3} b^{\dagger i_3} b^{i_4}) \rangle, \end{aligned} \quad (\text{E2})$$

where the superscript Γ denotes partial transposition applied here for the second mode. This relation between $\mathcal{M}_N^{\text{org}}$ and \mathcal{M}_N^Γ is a key observation of Ref. [43]. Let $\mathcal{M}_{N,(r_1,r_2,\dots,r_n)}$ denote the $n \times n$ submatrix of \mathcal{M}_N having \mathcal{M}_{r_i,r_j} elements. The Shchukin-Vogel criteria are based on the following Sylvester's theorem [44]: \mathcal{M}_N is *positive semidefinite* if and only if all its *principal minors* are non-negative, i.e., $\det \mathcal{M}_{N,(r_1,r_2,\dots,r_n)} \geq 0$. Thus, the Shchukin-Vogel criteria correspond to the positive-partial-transposition-based Peres-Horodecki criterion, but formulated in terms of the matrix

moments as [43,44]

$$\begin{aligned} \rho \text{ is PPT} &\Leftrightarrow \forall N, \forall \{r_k\} : \det \mathcal{M}_{N,(r_1,r_2,\dots,r_n)}^\Gamma \geq 0, \\ \rho \text{ is NPT} &\Leftrightarrow \exists N, \exists \{r_k\} : \det \mathcal{M}_{N,(r_1,r_2,\dots,r_n)}^\Gamma < 0, \end{aligned} \quad (\text{E3})$$

where $1 \leq r_1 < r_2 < \dots < r_n \leq N$, $n = 1, 2, \dots, N$, and PPT (NPT) stands for positive (nonpositive) states under partial transposition. Many popular entanglement criteria can be derived from the Shchukin-Vogel criteria [43,50], including the Hillery-Zubairy inequalities, which below are recalled and applied to the GWSs.

2. Hierarchy of the Hillery-Zubairy entanglement criteria

The Hillery-Zubairy (HZ) entanglement criteria for nonuniversal detection of two-mode entanglement read [100]

$$H_1(\rho) \equiv \langle n_1 n_2 \rangle - |\langle ab^\dagger \rangle|^2 < 0, \quad (\text{E4})$$

$$H_2(\rho) \equiv \langle n_1 \rangle \langle n_2 \rangle - |\langle ab \rangle|^2 < 0, \quad (\text{E5})$$

where $n_1 = a^\dagger a$ and $n_2 = b^\dagger b$. Thus, if $H_1(\rho) < 0$ or $H_2(\rho) < 0$ then ρ is entangled. The criteria are simple and useful witnesses of entanglement and have already been experimentally tested in a number of setups (see, e.g., [101]). These two criteria can be derived from the Shchukin-Vogel criteria by calculating

$$H_n(\rho) = \det \mathcal{M}_n^\Gamma \quad (\text{E6})$$

for

$$\mathcal{M}_1^{\text{org}} = \begin{bmatrix} 1 & \langle ab \rangle \\ \langle a^\dagger b^\dagger \rangle & \langle n_1 n_2 \rangle \end{bmatrix}, \quad \mathcal{M}_1^\Gamma = \begin{bmatrix} 1 & \langle ab^\dagger \rangle \\ \langle a^\dagger b \rangle & \langle n_1 n_2 \rangle \end{bmatrix} \quad (\text{E7})$$

and

$$\mathcal{M}_2^{\text{org}} = \begin{bmatrix} \langle n_1 \rangle & \langle a^\dagger b \rangle \\ \langle ab^\dagger \rangle & \langle n_2 \rangle \end{bmatrix}, \quad \mathcal{M}_2^\Gamma = \begin{bmatrix} \langle n_1 \rangle & \langle a^\dagger b^\dagger \rangle \\ \langle ab \rangle & \langle n_2 \rangle \end{bmatrix}, \quad (\text{E8})$$

respectively. To analyze the HZ criteria on the same footing as the discussed measures of quantum correlations, one can redefine H_n to be the HZ witnesses

$$\bar{H}_n = \max\{0, -H_n\}. \quad (\text{E9})$$

Let us now analyze in detail the hierarchy and effectiveness of these criteria in detecting the entanglement of the GWSs compared to the true measures of entanglement and other correlations. We find the HZ witnesses for the original GWSs,

$$\bar{H}_1(\rho_{\text{GW}}) = \max\{0, -\frac{1}{4}[1 + p(3 - 4q)]\} = 0, \quad (\text{E10})$$

$$\bar{H}_2(\rho_{\text{GW}}) = \max\{0, p^2 q \bar{q} - \frac{1}{4}(1 + p - 2pq)^2\}, \quad (\text{E11})$$

where $\bar{q} = 1 - q$. It can be seen that $\bar{H}_1(\rho_{\text{GW}})$ is useless in detecting the entanglement of the GWSs; however, $\bar{H}_2(\rho_{\text{GW}})$ can be nonzero. Thus, it detects entanglement for the GWSs corresponding to the blue-line-filled area in Fig. 9(a). The threshold (border) curve, as a function of the superposition parameter q in $\rho_{\text{GW}}(p, q)$, corresponds to the smallest allowed values of the mixing parameter p , for which the entanglement

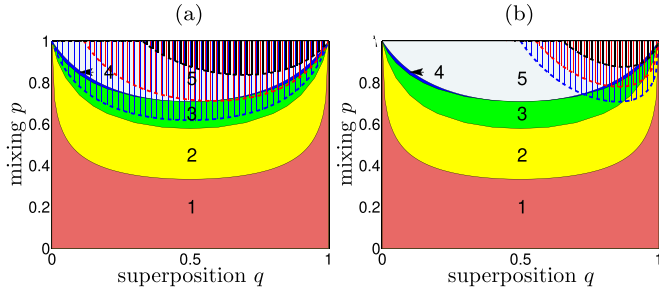


FIG. 9. Hierarchy of criteria versus the CC hierarchy for the GWSs. Specifically, the criterion hierarchy is based on different nonuniversal witnesses for a given class of quantum correlation, while the CC hierarchy reveals different types of correlations determined by their measures or universal witnesses. This is shown here by the example of nonuniversal entanglement witnesses using the (a) first and (b) second HZ witnesses. The color regions reveal the CC hierarchy, as in Fig. 6(a), while the areas filled with parallel lines show the criterion hierarchy. The latter areas determine the allowed values of the mixing parameter p and the superposition parameter q for the locally rotated GWSs, $\rho_\phi(p, q)$, for which entanglement can be revealed by the corresponding HZ witnesses: (a) $\bar{H}_1(\rho_\phi)$ for $\phi = \pi$ (area filled with blue lines), $\phi = 0.8\pi$ (red-line area), and $\phi = 0.7\pi$ (black-line area) and (b) $\bar{H}_2(\rho_\phi)$ for $\phi = 0$ (blue-line-filled area), $\phi = 0.2$ (red-line area), and $\phi = 0.3$ (black-line-filled area). For $\phi = \pi/2$ neither of the HZ witnesses can detect the entanglement of the GWSs. The dashed curves are obtained from the analytical formulas in Eqs. (E12), (E15), (E18), and (E19).

of the GWSs can be detected. This threshold is shown by the blue dashed curve in this figure and is given by

$$p_{H_2}(q) = 1/[2(q + \sqrt{q\bar{q}}) - 1] \quad (\text{E12})$$

for $q \in [\frac{1}{2}, 1]$. Let us now apply the Pauli operator σ_1 (the NOT gate) to the second qubit in the GWS, which results in the state $\rho_X = (I \otimes \sigma_1)\rho_{\text{GW}}(I \otimes \sigma_1)$. Note that the local unitary operation does not change entanglement measures, but of course it can change entanglement witnesses, which is the case for the HZ criteria. Indeed, this local transformation results in the HZ witnesses

$$\bar{H}_1(\rho_X) = \max \left\{ 0, p^2 q \bar{q} - \frac{1}{4} \bar{p} \right\}, \quad (\text{E13})$$

$$\bar{H}_2(\rho_X) = \max \left\{ 0, -\frac{1}{4}(1 - p^2) - p^2 q \bar{q} \right\} = 0, \quad (\text{E14})$$

where $\bar{p} = 1 - p$. It can be seen that the sensitivities of the HZ witnesses are exchanged for ρ_X compared to ρ_{GW} . The second criterion cannot detect entanglement, while the first reveals entanglement of some GWSs corresponding to those shown in the blue-line-filled area in Fig. 9(b). Analogously to Eq. (E12), the threshold curve for the first HZ witness for $\rho_X(p, q)$ is given by

$$p_{H_1, X}(q) = 2/[1 + \sqrt{1 + 16q\bar{q}}] \quad (\text{E15})$$

for $q \in [0, 1]$. Now let us apply an arbitrary rotation along the y axis of the second qubit in the GWSs. Thus, we transform ρ_{GW} into $\rho_\phi = [I \otimes R_Y(\phi)]\rho_{\text{GW}}[I \otimes R_Y^\dagger(\phi)]$, where the rotation is described by $R_Y(\phi) = [c, -s; s, c]$, with $c = \cos(\phi/2)$

and $s = \sin(\phi/2)$. The HZ witnesses for the locally rotated GWSs read

$$\bar{H}_1(\rho_\phi) = \max \left\{ 0, -\frac{1}{4}[c^2[1 + p(3 - 4q)] + s^2(\bar{p} - 4s^2 p^2 q \bar{q})] \right\}, \quad (\text{E16})$$

$$\bar{H}_2(\rho_\phi) = \max \left\{ 0, c^4 p^2 q \bar{q} - \frac{1}{4} f_+ (c^2 f_+ + s^2 f_-) \right\}, \quad (\text{E17})$$

where $f_\pm = 1 \pm p(1 - 2q)$. The threshold curves for the HZ witnesses applied to $\rho_\phi(p, q)$ are given by

$$p_{H_1}(q, \phi) = (f_1 + \sqrt{f_1^2 + 2f_2})f_2^{-1}, \quad (\text{E18})$$

$$p_{H_2}(q, \phi) = 2/[\sqrt{f} + 2(1 + C_1)q - C_1 - 1], \quad (\text{E19})$$

which are physically meaningful only in the regions of q for a given ϕ such that $p_{H_n}(q, \phi) \in [0, 1]$ ($n = 1, 2$). Here $f = (1 - C_1)^2(1 - 2q)^2 + 2(4C_1 + C_2 + 3)q\bar{q}$, with $C_n = \cos(n\phi)$, $f_1 = c^2(3 - 4q) - s^2$, and $f_2 = 8q\bar{q}s^4$. As seen in Fig. 9, the lowest value of q for which the entanglement of the GWSs can be detected via the HZ witness $\bar{H}_1(\rho_\phi)$ [$\bar{H}_2(\rho_\phi)$] is 0 ($\frac{1}{2}$) for $\phi = \pi$ ($\phi = 0$). For both HZ witnesses, the largest allowed value of q is equal to 1.

Figure 9 shows a comparison of the two approaches to analyze a hierarchy of quantum correlations, i.e., the criterion hierarchy, which is based on the HZ witnesses, and the CC hierarchy, which is based on the discussed quantum correlation measures. Any good measure of entanglement results in the same CC hierarchy for the GWSs, while the criterion hierarchy depends on the applied nonuniversal witnesses and can reveal only a subset of the entangled GWSs, which correspond to regimes 2–5. This figure explains our motivation of experimentally demonstrating in detail only the CC hierarchy instead of the hierarchy based on the HZ witnesses, or using other either sufficient or necessary conditions of quantum correlations. Unfortunately, by contrast to such a hierarchy of criteria, it is experimentally challenging to reveal such a CC hierarchy for the GWSs without QST.

3. Quantum state tomography via moments of annihilation and creation operators

Here we give an example showing that some very limited additional measurements on a given state can supplement a partial state reconstruction into a full QST.

We recall that a general single-mode density matrix ρ of a bosonic field can be reconstructed from the following moments of the annihilation and creation operators via the formula [102]

$$\langle m_1 | \rho | m_2 \rangle = \sum_{j=0}^{\infty} \frac{1}{j! \sqrt{m_1! m_2!}} \langle (a^\dagger)^{m_2+j} a^{m_1+j} \rangle. \quad (\text{E20})$$

Note that this formula can be divergent for some states of the radiation field including thermal field with the mean photon number $\langle n \rangle \geq 1$. However, for finite-dimensional states, the above sum becomes finite. In particular, a two-mode version

of Eq. (E20) leads to the moment-based representation

$$\begin{bmatrix} f & \langle b^\dagger \rangle - \langle n_1 b^\dagger \rangle & \langle a^\dagger \rangle - \langle a^\dagger n_2 \rangle & \langle a^\dagger b^\dagger \rangle \\ \langle b \rangle - \langle n_1 b \rangle & \langle n_2 \rangle - \langle n_1 n_2 \rangle & \langle a^\dagger b \rangle & \langle a^\dagger n_2 \rangle \\ \langle a \rangle - \langle a n_2 \rangle & \langle a b^\dagger \rangle & \langle n_1 \rangle - \langle n_1 n_2 \rangle & \langle n_1 b^\dagger \rangle \\ \langle a b \rangle & \langle a n_2 \rangle & \langle n_1 b \rangle & \langle n_1 n_2 \rangle \end{bmatrix} \quad (\text{E21})$$

of a general two-qubit state ρ , where $f = 1 - \langle n_1 \rangle - \langle n_2 \rangle + \langle n_1 n_2 \rangle$ and the annihilation operator $a = a_1$ (and analogously

$b = a_2$) is simply $a = \sigma_- = [0, 1; 0, 0]$, i.e., the qubit lowering operator. Thus, an arbitrary two-qubit state can be completely reconstructed by measuring only the moments $\langle n_i \rangle$, $\langle n_1 n_2 \rangle$, $\langle a_i \rangle$, $\langle n_i a_{2-i} \rangle$, $\langle a_1 a_2 \rangle$, and $\langle a_1 a_2^\dagger \rangle$ for $i = 1, 2$.

Note that experimental implementations of the HZ witnesses require measuring $\langle n_i \rangle$, $\langle n_1 n_2 \rangle$, $\langle a_1 a_2 \rangle$, and $\langle a_1 a_2^\dagger \rangle$. Thus, by measuring additionally only the moments $\langle a_i \rangle$ and $\langle n_i a_{2-i} \rangle$, one can collect all the information required for a complete QST, with which one can thus calculate any properties of an experimentally reconstructed two-qubit state.

-
- [1] A. Einstein, B. Podolsky, and N. Rosen, Can quantum-mechanical description of physical reality be considered complete? *Phys. Rev.* **47**, 777 (1935).
- [2] E. Schrödinger, Discussion of probability relations between separated systems, *Math. Proc. Cambridge* **31**, 555 (1935).
- [3] E. Schrödinger, Probability relations between separated systems, *Math. Proc. Cambridge* **32**, 446 (1936).
- [4] J. S. Bell, On the Einstein Podolsky Rosen paradox, *Physics* **1**, 195 (1964).
- [5] R. Horodecki, P. Horodecki, M. Horodecki, and K. Horodecki, Quantum entanglement, *Rev. Mod. Phys.* **81**, 865 (2009).
- [6] N. Brunner, D. Cavalcanti, S. Pironio, V. Scarani, and S. Wehner, Bell nonlocality, *Rev. Mod. Phys.* **86**, 419 (2014).
- [7] D. Cavalcanti and P. Skrzypczyk, Quantum steering: A review with focus on semidefinite programming, *Rep. Prog. Phys.* **80**, 024001 (2017).
- [8] R. Uola, A. C. S. Costa, H. C. Nguyen, and O. Gühne, Quantum steering, *Rev. Mod. Phys.* **92**, 015001 (2020).
- [9] J. F. Clauser, M. A. Horne, A. Shimony, and R. A. Holt, Proposed Experiment to Test Local Hidden-Variable Theories, *Phys. Rev. Lett.* **23**, 880 (1969).
- [10] H. M. Wiseman, S. J. Jones, and A. C. Doherty, Steering, Entanglement, Nonlocality, and the Einstein-Podolsky-Rosen Paradox, *Phys. Rev. Lett.* **98**, 140402 (2007).
- [11] R. F. Werner, Quantum states with Einstein-Podolsky-Rosen correlations admitting a hidden-variable model, *Phys. Rev. A* **40**, 4277 (1989).
- [12] Y.-Y. Zhao, H.-Y. Ku, S.-L. Chen, H.-B. Chen, F. Nori, G.-Y. Xiang, C.-F. Li, G.-C. Guo, and Y.-N. Chen, Experimental demonstration of measurement-device-independent measure of quantum steering, *npj Quantum Inf.* **6**, 77 (2020).
- [13] H.-Y. Ku, S.-L. Chen, N. Lambert, Y.-N. Chen, and F. Nori, Hierarchy in temporal quantum correlations, *Phys. Rev. A* **98**, 022104 (2018).
- [14] J. F. Fitzsimons, J. A. Jones, and V. Vedral, Quantum correlations which imply causation, *Sci. Rep.* **5**, 18281 (2015).
- [15] T. Fritz, Quantum correlations in the temporal Clauser-Horne-Shimony-Holt (CHSH) scenario, *New J. Phys.* **12**, 083055 (2010).
- [16] Y.-N. Chen, C.-M. Li, N. Lambert, S.-L. Chen, Y. Ota, G.-Y. Chen, and F. Nori, Temporal steering inequality, *Phys. Rev. A* **89**, 032112 (2014).
- [17] K. Bartkiewicz, A. Černoch, K. Lemr, A. Miranowicz, and F. Nori, Temporal steering and security of quantum key distribution with mutually unbiased bases against individual attacks, *Phys. Rev. A* **93**, 062345 (2016).
- [18] R. T. Thew and W. J. Munro, Mixed state entanglement: Manipulating polarization-entangled photons, *Phys. Rev. A* **64**, 022320 (2001).
- [19] C. Zhang, Preparation of polarization-entangled mixed states of two photons, *Phys. Rev. A* **69**, 014304 (2004).
- [20] T.-C. Wei, J. B. Altepeter, D. Branning, P. M. Goldbart, D. F. V. James, E. Jeffrey, P. G. Kwiat, S. Mukhopadhyay, and N. A. Peters, Synthesizing arbitrary two-photon polarization mixed states, *Phys. Rev. A* **71**, 032329 (2005).
- [21] G. Lima, F. Torres-Ruiz, L. Neves, A. Delgado, C. Saavedra, and S. Pádua, Generating mixtures of spatial qubits, *Opt. Commun.* **281**, 5058 (2008).
- [22] A. Ling, P. Y. Han, A. Lamas-Linares, and C. Kurtsiefer, Preparation of Bell states with controlled white noise, *Laser Phys.* **16**, 1140 (2006).
- [23] T.-J. Liu, C.-Y. Wang, J. Li, and Q. Wang, Experimental preparation of an arbitrary tunable Werner state, *Europhys. Lett.* **119**, 14002 (2017).
- [24] G. Puentes, D. Voigt, A. Aiello, and J. P. Woerdman, Tunable spatial decoherers for polarization-entangled photons, *Opt. Lett.* **31**, 2057 (2006).
- [25] A. G. White, D. F. V. James, W. J. Munro, and P. G. Kwiat, Exploring Hilbert space: Accurate characterization of quantum information, *Phys. Rev. A* **65**, 012301 (2001).
- [26] Y.-S. Zhang, Y.-F. Huang, C.-F. Li, and G.-C. Guo, Experimental preparation of the Werner state via spontaneous parametric down-conversion, *Phys. Rev. A* **66**, 062315 (2002).
- [27] C. Cinelli, G. Di Nepi, F. De Martini, M. Barbieri, and P. Mataloni, Parametric source of two-photon states with a tunable degree of entanglement and mixing: Experimental preparation of Werner states and maximally entangled mixed states, *Phys. Rev. A* **70**, 022321 (2004).
- [28] M. Caminati, F. De Martini, R. Perris, F. Sciarrino, and V. Secondi, Nonseparable Werner states in spontaneous parametric down-conversion, *Phys. Rev. A* **73**, 032312 (2006).
- [29] G. Puentes, A. Aiello, D. Voigt, and J. P. Woerdman, Entangled mixed-state generation by twin-photon scattering, *Phys. Rev. A* **75**, 032319 (2007).
- [30] A. Aiello, G. Puentes, D. Voigt, and J. P. Woerdman, Maximally entangled mixed-state generation via local operations, *Phys. Rev. A* **75**, 062118 (2007).
- [31] G. Brida, M. Genovese, M. V. Chekhova, and L. A. Krivitsky, Tailoring polarization entanglement in anisotropy-compensated spontaneous parametric down-conversion, *Phys. Rev. A* **77**, 015805 (2008).

- [32] N. A. Peters, J. B. Altepeter, D. Branning, E. R. Jeffrey, T.-C. Wei, and P. G. Kwiat, Maximally Entangled Mixed States: Creation and Concentration, *Phys. Rev. Lett.* **92**, 133601 (2004).
- [33] M. Barbieri, F. De Martini, G. Di Nepi, and P. Mataloni, Generation and Characterization of Werner States and Maximally Entangled Mixed States by a Universal Source of Entanglement, *Phys. Rev. Lett.* **92**, 177901 (2004).
- [34] P. G. Kwiat, A. J. Berglund, J. B. Altepeter, and A. G. White, Experimental verification of decoherence-free subspaces, *Science* **290**, 498 (2000).
- [35] W. J. Munro, D. F. V. James, A. G. White, and P. G. Kwiat, Maximizing the entanglement of two mixed qubits, *Phys. Rev. A* **64**, 030302(R) (2001).
- [36] Y.-C. Jeong, J.-C. Lee, and Y.-H. Kim, Experimental implementation of a fully controllable depolarizing quantum operation, *Phys. Rev. A* **87**, 014301 (2013).
- [37] K. Lemr, K. Bartkiewicz, and A. Černoč, Experimental measurement of collective nonlinear entanglement witness for two qubits, *Phys. Rev. A* **94**, 052334 (2016).
- [38] M. Gavenda, A. Černoč, J. Soubusta, M. Dušek, and R. Filip, Knowledge excess duality and violation of Bell inequalities: theory and experiment, *Mod. Phys. Lett. B* **19**, 195 (2005).
- [39] A. Aspect, J. Dalibard, and G. Roger, Experimental Test of Bell's Inequalities Using Time-Varying Analyzers, *Phys. Rev. Lett.* **49**, 1804 (1982).
- [40] B. G. Christensen *et al.*, Detection-Loophole-Free Test of Quantum Nonlocality, and Applications, *Phys. Rev. Lett.* **111**, 130406 (2013).
- [41] M. Giustina *et al.*, Significant-Loophole-Free Test of Bell's Theorem with Entangled Photons, *Phys. Rev. Lett.* **115**, 250401 (2015).
- [42] B. Hensen *et al.*, Loophole-free Bell inequality violation using electron spins separated by 1.3 kilometres, *Nature (London)* **526**, 682 (2015).
- [43] E. Shchukin and W. Vogel, Inseparability Criteria for Continuous Bipartite Quantum States, *Phys. Rev. Lett.* **95**, 230502 (2005).
- [44] A. Miranowicz and M. Piani, Comment on "Inseparability Criteria for Continuous Bipartite Quantum States", *Phys. Rev. Lett.* **97**, 058901 (2006).
- [45] A. Miranowicz, M. Piani, P. Horodecki, and R. Horodecki, Inseparability criteria based on matrices of moments, *Phys. Rev. A* **80**, 052303 (2009).
- [46] I. Kogias, P. Skrzypczyk, D. Cavalcanti, A. Acín, and G. Adesso, Hierarchy of Steering Criteria Based on Moments for All Bipartite Quantum Systems, *Phys. Rev. Lett.* **115**, 210401 (2015).
- [47] M. Navascués, S. Pironio, and A. Acín, Bounding the Set of Quantum Correlations, *Phys. Rev. Lett.* **98**, 010401 (2007).
- [48] T. Richter and W. Vogel, Nonclassicality of Quantum States: A Hierarchy of Observable Conditions, *Phys. Rev. Lett.* **89**, 283601 (2002).
- [49] W. Vogel, Nonclassical Correlation Properties of Radiation Fields, *Phys. Rev. Lett.* **100**, 013605 (2008).
- [50] A. Miranowicz, M. Bartkowiak, X. Wang, Y.-x. Liu, and F. Nori, Testing nonclassicality in multimode fields: A unified derivation of classical inequalities, *Phys. Rev. A* **82**, 013824 (2010).
- [51] K. Życzkowski, P. Horodecki, A. Sanpera, and M. Lewenstein, Volume of the set of separable states, *Phys. Rev. A* **58**, 883 (1998).
- [52] M. Horodecki, P. Horodecki, and R. Horodecki, Separability of mixed states: Necessary and sufficient conditions, *Phys. Lett. A* **223**, 1 (1996).
- [53] K. Audenaert, M. B. Plenio, and J. Eisert, Entanglement Cost under Positive-Partial-Transpose-Preserving Operations, *Phys. Rev. Lett.* **90**, 027901 (2003).
- [54] S. Ishizaka, Binegativity and geometry of entangled states in two qubits, *Phys. Rev. A* **69**, 020301(R) (2004).
- [55] C. Eltschka and J. Siewert, Negativity as an Estimator of Entanglement Dimension, *Phys. Rev. Lett.* **111**, 100503 (2013).
- [56] W. K. Wootters, Entanglement of Formation of an Arbitrary State of Two Qubits, *Phys. Rev. Lett.* **80**, 2245 (1998).
- [57] J. K. Asbóth, J. Calsamiglia, and H. Ritsch, Computable Measure of Nonclassicality for Light, *Phys. Rev. Lett.* **94**, 173602 (2005).
- [58] A. Miranowicz, K. Bartkiewicz, A. Pathak, J. Peřina, Jr., Y.-N. Chen, and F. Nori, Statistical mixtures of states can be more quantum than their superpositions: Comparison of nonclassicality measures for single-qubit states, *Phys. Rev. A* **91**, 042309 (2015).
- [59] A. Miranowicz, K. Bartkiewicz, N. Lambert, Y.-N. Chen, and F. Nori, Increasing relative nonclassicality quantified by standard entanglement potentials by dissipation and unbalanced beam splitting, *Phys. Rev. A* **92**, 062314 (2015).
- [60] K. Bartkiewicz, P. Horodecki, K. Lemr, A. Miranowicz, and K. Życzkowski, Method for universal detection of two-photon polarization entanglement, *Phys. Rev. A* **91**, 032315 (2015).
- [61] R. Augusiak, M. Demianowicz, and P. Horodecki, Universal observable detecting all two-qubit entanglement and determinant-based separability tests, *Phys. Rev. A* **77**, 030301(R) (2008).
- [62] P. Skrzypczyk, M. Navascués, and D. Cavalcanti, Quantifying Einstein-Podolsky-Rosen Steering, *Phys. Rev. Lett.* **112**, 180404 (2014).
- [63] M. Piani and J. Watrous, Necessary and Sufficient Quantum Information Characterization of Einstein-Podolsky-Rosen Steering, *Phys. Rev. Lett.* **114**, 060404 (2015).
- [64] H.-Y. Ku, S.-L. Chen, C. Budroni, A. Miranowicz, Y.-N. Chen, and F. Nori, Einstein-Podolsky-Rosen steering: Its geometric quantification and witness, *Phys. Rev. A* **97**, 022338 (2018).
- [65] S.-L. Chen, N. Lambert, C.-M. Li, A. Miranowicz, Y.-N. Chen, and F. Nori, Quantifying Non-Markovianity with Temporal Steering, *Phys. Rev. Lett.* **116**, 020503 (2016).
- [66] H.-Y. Ku, S.-L. Chen, H.-B. Chen, N. Lambert, Y.-N. Chen, and F. Nori, Temporal steering in four dimensions with applications to coupled qubits and magnetoreception, *Phys. Rev. A* **94**, 062126 (2016).
- [67] S.-L. Chen, N. Lambert, C.-M. Li, G.-Y. Chen, Y.-N. Chen, A. Miranowicz, and F. Nori, Spatio-temporal steering for testing nonclassical correlations in quantum networks, *Sci. Rep.* **7**, 3728 (2017).
- [68] F. Hirsch, M. T. Quintino, T. Vértesi, M. F. Pusey, and N. Brunner, Algorithmic Construction of Local Hidden Variable Models for Entangled Quantum States, *Phys. Rev. Lett.* **117**, 190402 (2016).

- [69] M. Fillettaz, F. Hirsch, S. Designolle, and N. Brunner, Algorithmic construction of local models for entangled quantum states: Optimization for two-qubit states, *Phys. Rev. A* **98**, 022115 (2018).
- [70] R. Horodecki, P. Horodecki, and M. Horodecki, Violating Bell inequality by mixed states: Necessary and sufficient condition, *Phys. Lett. A* **200**, 340 (1995).
- [71] R. Horodecki, Two-spin-1/2 mixtures and Bell's inequalities, *Phys. Lett. A* **210**, 223 (1996).
- [72] C. H. Bennett, D. P. DiVincenzo, C. A. Fuchs, T. Mor, E. Rains, P. W. Shor, J. A. Smolin, and W. K. Wootters, Quantum nonlocality without entanglement, *Phys. Rev. A* **59**, 1070 (1999).
- [73] S. Popescu, Bell's Inequalities versus Teleportation: What is Nonlocality? *Phys. Rev. Lett.* **72**, 797 (1994).
- [74] A. Miranowicz, Violation of Bell inequality and entanglement of decaying Werner states, *Phys. Lett. A* **327**, 272 (2004).
- [75] K. Bartkiewicz, K. Lemr, A. Černoč, and A. Miranowicz, Bell nonlocality and fully entangled fraction measured in an entanglement-swapping device without quantum state tomography, *Phys. Rev. A* **95**, 030102(R) (2017).
- [76] A. C. Elitzur, S. Popescu, and D. Rohrlich, Quantum nonlocality for each pair in an ensemble, *Phys. Lett. A* **162**, 25 (1992).
- [77] J. Barrett, A. Kent, and S. Pironio, Maximally Nonlocal and Monogamous Quantum Correlations, *Phys. Rev. Lett.* **97**, 170409 (2006).
- [78] L. Aolita, R. Gallego, A. Acín, A. Chiuri, G. Vallone, P. Mataloni, and A. Cabello, Fully nonlocal quantum correlations, *Phys. Rev. A* **85**, 032107 (2012).
- [79] S. Ghosh, G. Kar, A. Sen(De), and U. Sen, Mixedness in the Bell violation versus entanglement of formation, *Phys. Rev. A* **64**, 044301 (2001).
- [80] T.-C. Wei, K. Nemoto, P. M. Goldbart, P. G. Kwiat, W. J. Munro, and F. Verstraete, Maximal entanglement versus entropy for mixed quantum states, *Phys. Rev. A* **67**, 022110 (2003).
- [81] P. G. Kwiat, E. Waks, A. G. White, I. Appelbaum, and P. H. Eberhard, Ultrabright source of polarization-entangled photons, *Phys. Rev. A* **60**, R773 (1999).
- [82] E. Halenková, A. Černoč, K. Lemr, J. Soubusta, and S. Drusová, Experimental implementation of the multifunctional compact two-photon state analyzer, *Appl. Opt.* **51**, 474 (2012).
- [83] K. Banaszek, G. M. D'Ariano, M. G. A. Paris, and M. F. Sacchi, Maximum-likelihood estimation of the density matrix, *Phys. Rev. A* **61**, 010304(R) (1999).
- [84] D. F. V. James, P. G. Kwiat, W. J. Munro, and A. G. White, Measurement of qubits, *Phys. Rev. A* **64**, 052312 (2001).
- [85] Z. Hradil, J. Řeháček, J. Fiurášek, and M. Ježek, in *Quantum State Estimation*, edited by M. Paris and J. Řeháček, Lecture Notes in Physics Vol. 649 (Springer, Berlin, 2004), Chap. 3, pp. 266–290.
- [86] C. Sanderson and R. Curtin, Armadillo: A template-based C++ library for linear algebra, *J. Open Source Softw.* **1**, 26 (2016).
- [87] C. Sanderson and R. Curtin, in *Mathematical Software – ICMS 2018*, edited by J. Davenport, M. Kauers, G. Labahn, and J. Urban, Lecture Notes in Computer Science Vol. 10931 (Springer, Cham, 2018), pp. 422–430.
- [88] See Supplemental Material at <http://link.aps.org/supplemental/10.1103/PhysRevA.104.062436> for the density matrices for our experimental GWSs and Werner states.
- [89] P. Girdhar and E. G. Cavalcanti, All two-qubit states that are steerable via Clauser-Horne-Shimony-Holt-type correlations are Bell nonlocal, *Phys. Rev. A* **94**, 032317 (2016).
- [90] E. G. Cavalcanti, C. J. Foster, M. Fuwa, and H. M. Wiseman, Analog of the Clauser-Horne-Shimony-Holt inequality for steering, *J. Opt. Soc. Am. B* **32**, A74 (2015).
- [91] A. C. S. Costa and R. M. Angelo, Quantification of Einstein-Podolsky-Rosen steering for two-qubit states, *Phys. Rev. A* **93**, 020103(R) (2016).
- [92] Č. Brukner, Quantum causality, *Nat. Phys.* **10**, 259 (2014).
- [93] K. Bartkiewicz, J. Beran, K. Lemr, M. Norek, and A. Miranowicz, Quantifying entanglement of a two-qubit system via measurable and invariant moments of its partially transposed density matrix, *Phys. Rev. A* **91**, 022323 (2015).
- [94] K. Bartkiewicz, G. Chiriac, and K. Lemr, Direct method for measuring and witnessing quantum entanglement of arbitrary two-qubit states through Hong-Ou-Mandel interference, *Phys. Rev. A* **95**, 022331 (2017).
- [95] C. H. Bennett, D. P. DiVincenzo, J. A. Smolin, and W. K. Wootters, Mixed-state entanglement and quantum error correction, *Phys. Rev. A* **54**, 3824 (1996).
- [96] E. G. Cavalcanti, S. J. Jones, H. M. Wiseman, and M. D. Reid, Experimental criteria for steering and the Einstein-Podolsky-Rosen paradox, *Phys. Rev. A* **80**, 032112 (2009).
- [97] M. Grant and S. Boyd, *CVX: Matlab software for disciplined convex programming*, <http://cvxr.com/cvx> (CVX Research, Austin, 2012).
- [98] D. Cavalcanti, L. Guerini, R. Rabelo, and P. Skrzypczyk, General Method for Constructing Local Hidden Variable Models for Entangled Quantum States, *Phys. Rev. Lett.* **117**, 190401 (2016).
- [99] E. V. Shchukin and W. Vogel, Nonclassical moments and their measurement, *Phys. Rev. A* **72**, 043808 (2005).
- [100] M. Hillery and M. S. Zubairy, Entanglement Conditions for Two-Mode States, *Phys. Rev. Lett.* **96**, 050503 (2006).
- [101] R. M. Gomes, A. Salles, F. Toscano, P. H. S. Ribeiro, and S. P. Walborn, Quantum entanglement beyond Gaussian criteria, *Proc. Natl. Acad. Sci. USA* **106**, 21517 (2009).
- [102] A. Wünsche, Tomographic reconstruction of the density operator from its normally ordered moments, *Phys. Rev. A* **54**, 5291 (1996).